HYDRODYNAMICS AND MASS TRANSFER IN A NOVEL MULTI-AIRLIFTING MEMBRANE BIOREACTOR.

A THESIS SUBMITTED TO THE GRADUATE DIVISION OF
THE UNIVERSITY OF HAWAI'I IN PARTIAL FULFILLMENT OF
THE REQUIREMENTS FOR THE DEGREE OF

MASTER OF SCIENCE

IN

BIOENGINEERING

DECEMBER 2007

By
Zhe Xu

Thesis Committee:

Jian Yu, Chairperson
Stephen M. Masutani
Winston Su

We certify that we have read this thesis and that, in our opinion, it is satisfactory in scope, and quality as a thesis for the degree of Master of Science in Bioengineering.

THESIS COMMITTEE

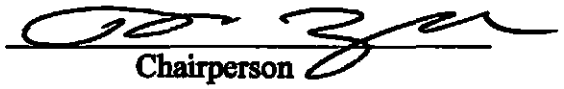

Chairperson

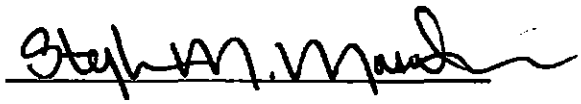

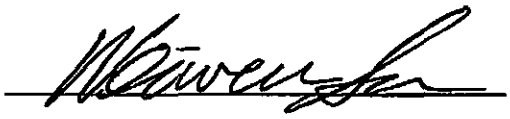

TABLE OF CONTENTS

Chapter 1. INTRODUCTION

1.1 Background

Nowadays, in order to relieve the environmental burden, more and more concerns are concentrated on how to maximally dispose the industrial organic waste. Meanwhile, it is expected to find a solution which can combine the waste treatment with the production of valuable products. In this way, the high cost of disposal procedures would be effectively cut down by adding extra value in it. The procedure of production of polyhydroxyalkanoates (PHAs) provides such a beneficial waste treatment which can be applied in various industries, especially in food processing industry where high cost of high BOD wastes treatment is involved (Yu and Si 2001).

By using different configurations of bioreactors, several new technologies have been developed demonstrating the feasibility of combining anaerobic digestion of food scraps with aerobic production of biodegradable thermoplastics, polyhydroxyalkanoates (PHAs). Yu and his coworkers (1999) reported the effects of superficial gas and liquid velocities on bed expansion, solid and gas hold-ups and specific oxygen mass transfer rate, k_La by using a type of porous glass beads for immobilization of microbial cells in a three-phase aerobic fluidized bed reactor (AFBR) with an external liquid circulation. This is the first attempt to combine the anaerobic/aerobic treatment

of wastewater to produce PHAs.

Later on, Du and Yu (2002) developed a new technique to connect the anaerobic reactor and the aerobic reactor through a tubular module of silicone rubber membrane or dialysis membrane. Their efforts yielded 72.6% (wt) PHAs in PHA-producing cells which was the highest polymer content achieved in waste treatment since their work were reported.

Although waste water process can get great benefits from PHAs production, the major barrier to widely apply the production of PHAs is their high price, which is more than 10 times higher than the price of synthetic counterparts, reported by Yu and Si (2001).

PHAs have attracted academic and industrial attention due to their potential use as biodegradable thermoplastics. The production cost can be significantly reduced by raising the scale as well as the productivity of bioreactors. Based on this, we investigate a mini-pilot scale bioreactor (60L), which is promising to be scaled up to 3000L for PHAs production at a reduced production cost.

In this work, a multiple airlifting membrane bioreactor (MAMBR) was designed, fabricated and investigated for operational hydrodynamics and mass transfers (as shown in Fig.1.1).

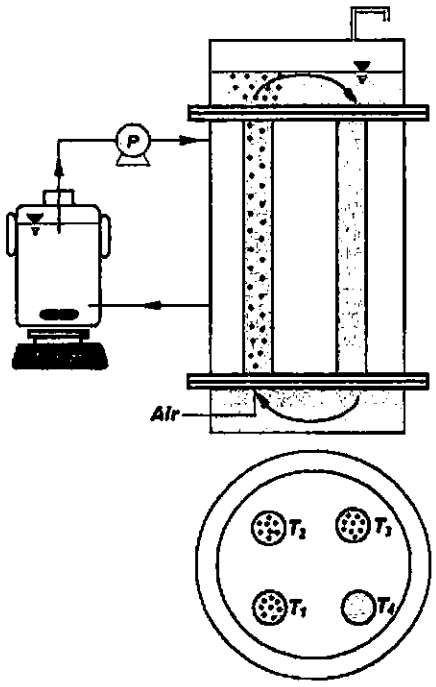

Fig. 1.1 Schematic diagram of the multi-airlifting membrane bioreactor (MAMBR)

The bioreactor could be operated with different numbers of risers (1 to 3) and downcomers (3 to 1), respectively, to give a control on overall mixing and mass transfer. In addition, the multiple risers and downcomers were micro-filtration filter tubes, allowing molecular diffusion of metabolic intermediates through the wall membranes. We report the results on hydrodynamics and mass transfer in this novel bioreactor, including the gas holdups in risers and downcomers, the superficial liquid velocities, the liquid circulation and mixing times, the oxygen mass transfer (k_La) in aerobic compartment, and the effective molecular diffusivities of lactic and acetic acids, two representative fermentative acids, across the membranes of

micro-filtration filters.

1.2 Hydrodynamics in pneumatically agitated bioreactors

Since the first airlifter was invented by Lefrancois about 50 years ago (1955), air-lifting reactors have found increasing applications in bioprocesses, because of many advantages such as simple structure, low energy consumption, good mixing and low shear stress to cells (Chisti & Moo-Young, 1987; Chisti 1989).

Airlift bioreactors are originally modified from one important type of bioreactors, the bubble columns that offer a simple structure without internals or moving parts, a high gas phase content, an excellent heat transfer capacity, a reasonable interphase mass transfer rate and good mixing properties at low energy consumption, as the gas phase serves the dual function of aeration and agitation. Airlifters, however, have additional advantages over bubble columns due to the higher overall liquid velocity and the higher intensity of turbulence which renders, for example, an increased heat and mass transfer capacity. Indeed, both the turbulent field in the liquid phase and the overall directionality of the flow impose a more uniform distribution of shear in airlifters. This explains why airlift reactors are preferentially used for animal cell culture where low shear is demanded.

Airlifters usually have two compartments -- a riser where gas is sparged to

give an upflow of fluids and a downcomer where little or no gas exists to give a net downflow of liquid. The difference in gas holdup between the two compartments is the driving force for a stable and defined fluid circulation and mixing in the bioreactor.

Airlift bioreactors can be divided into two classes namely, the internal loop airlift reactors (IL-ALR) and the external loop airlift reactors (EL-ALR) as shown in Fig.1.2.

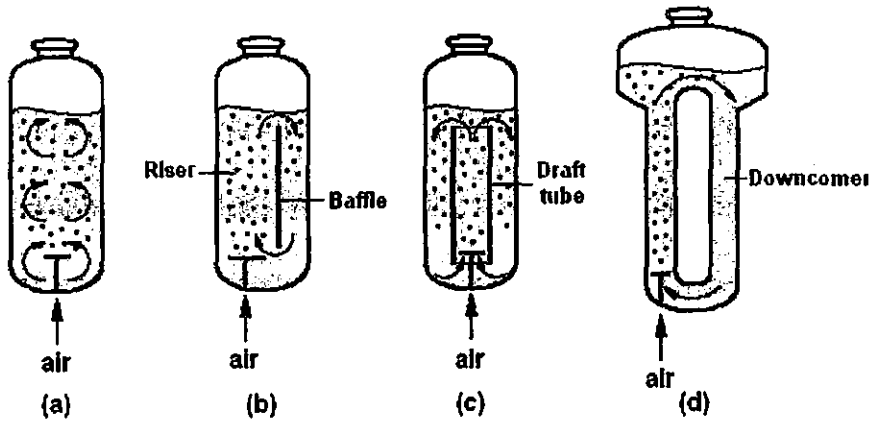

Fig.1.2. Schematic diagram of pneumatically agitated bioreactors. (a) bubble column; (b) split-cylinder internal-loop ALR; (c) draft-tube internal-loop ALR; (d) external loop ALR.

EL-ALRs differ considerably from IL-ALRs because they consist of two separate columns connected at the top and the bottom by two horizontal sections. The main difference is due to the presence of a separate gas disengagement section in EL-ALRs, which enables, if needed, complete degassing. As a consequence, EL-ALRs, which are often designed to operate with complete gas disengagement maximizes the liquid circulation and improves mixing and heat transfer in the reactor. In addition the external loop

facilitates temperature control in the reactor (Bentifraouine et al. 1997b).

Progress in biotechnology has been generating new biosystems that requires novel bioreactors for new metabolic products or improved yield and productivity. For instance, membrane bioreactors have been used for simultaneous cell cultivation and removal of the spent medium or metabolic inhibitors (Yang 2006). In some applications, aerobic and anaerobic cultures should work together for a complete biosynthesis or bioconversion (Yu and Si 2001). Although conventional bioreactors could be modified by adding external circulation lines equipped with pumps, micro-filters or centrifuges to meet the demands (Yu et al. 1999), the facility cost is high and continuous operation may have problems such as contamination, cell damage, and so on. Different airlifting configurations have been designed and investigated, but most of them are based on conventional structure of one riser and one downcomer (Bendjaballah et al. 1999; Benyahia and Jones 1997; Camarasa et al. 2001a; Choi 2002; Freitas et al. 2000; Kawase and Hashimoto 1996; Mohanty et al. 2006; Nikakhtari and Hill 2005; Vial et al. 2002).

One novel cascaded airlifting reactor was investigated by Bakker et al. (1994) for hydrolysis of sucrose to glucose and fructose using immobilized invertase (Figure 1.3). As proposed by the author, one advantage of cascaded airlift reactor over multiple separate units is the elimination of interconnecting pipework and pumps. In addition, a series of different reactions, aerobic and

anaerobic may be carried out within one vessel in the cascaded configuration. However, the reactor configuration is quite restrictive.

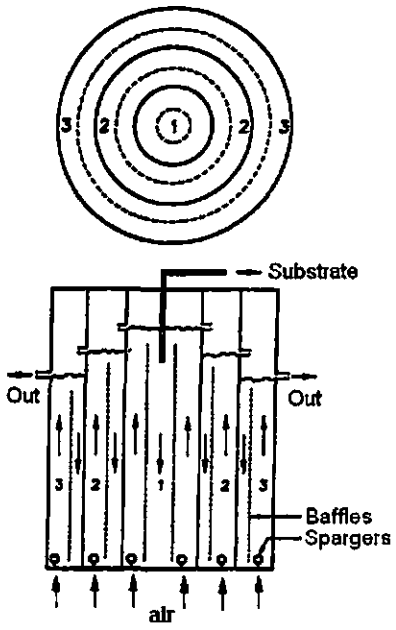

Fig. 1.3. Schematic diagram of Cascaded airlift reactor (Bakker et al. 1994)

Another unconventional airlift reactor was reported by Liu et al. (2000), as shown in Fig.1.4. The proposed reactor was composed of two risers and two downcomers which were connected by a gas-liquid separator at the top and a liquid container at the bottom. Both the separator and container were divided into two chambers with equal volume by a baffle and two gas spargers were mounted at the inlet of two risers. Like the cascaded reactor discussed above, the reactor investigated by Liu actually elongate both the lengths of the riser and downcomer comprised conventional reactor. Ratio of downcomer to riser cross sectional areas, which is one of the crucial factors that affect

performance of airlift reactors, was unfortunately not investigated.

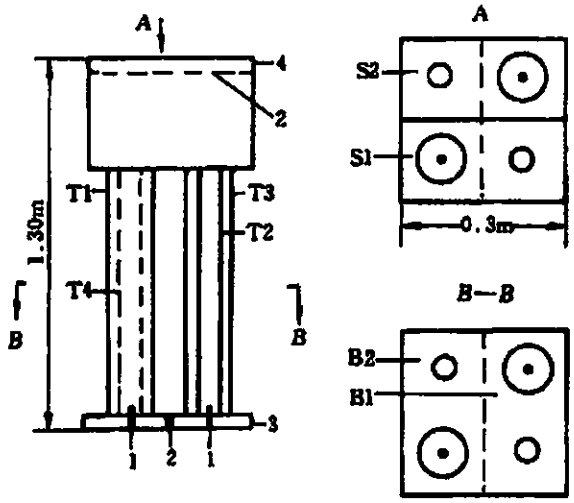

Fig. 1.4. Configuration of the multi-tube air-lift reactor (Liu et al. 2000). Symbols: 1, sparger; 2, baffle; 3, base box; 4, separator; B1, base box 1; B2, base box 2; S1, separator 1; S2, separator 2; T1, tube 1; T2, tube 2; T3, tube 3; T4, tube 4.

Compared to other pneumatically agitated bioreactors in industrial and environmental bioprocess, novel MAMBR not only shares all the advantages of common airlift reactors, but also possesses its unique assets:

- High mixing performance. The main difference between conventional bubble columns and the riser section of the external loop airlift reactor (EL-ALR) is that the range of liquid velocities in the EL-ALR is one to two orders of magnitude higher than that encountered in bubble columns.
- High mass transfer rate. The operational range of airlift reactors tends to be generally broader than that of bubble columns. Unlike in bubble

columns, the overall height (h_L) of liquid in airlift reactors affects k_La because the height strongly influence the liquid circulation velocity and, hence, the gas holdup

- Good heat transfer. Airlift systems are better than bubble columns in heat transfer capabilities.
- Low energy consumption. Compared to mechanically agitated vessels, airlift reactors require less power for attaining a given rate of gas–liquid mass transfer.
- Low shear rate as compared with stirred tanks, because of no moving parts.
- Simplified production processes. By combining aerobic and anaerobic reaction in a single reactor, complexity of multi-stage operating and extra cost on otherwise maintenance are greatly reduced.

Chapter 2. LITERATURE REVIEWS

From geometrical aspect, the tube-side of the MAMBR shares lots of similarities with external-loop airlift reactors (EL-ALR). Therefore, in order to effectively investigate the features of hydrodynamics and mass transfer inside MAMBR, it is necessary to comprehensively understand those of EL-ALR first.

In airlift bioreactors, given superficial gas velocity value, any variation of gas or liquid physical properties, downcomer connecting sections geometry, phase separation conditions, liquid volume, reactor height or gas distributing plate, generates a modification in liquid velocity and gas-holdup (Bentifraouine et al. 1997b). Therefore, in the following sections, important variables and factors that affect hydrodynamics and mass transfer of EL-ALR will be categorized and reviewed based on existing knowledge and previous investigations.

2.1 Gas holdup ε

Gas holdup is defined as the void fraction within the reactor or as the area occupied by the gas fraction divided by the cross-sectional area (Saez et al. 1998). Gas holdup can be further classified as "overall" gas holdup or "local" gas holdup according to different methods and locations of measurements(Petersen and Margaritis 2001).

2.1.1 Prediction equation of gas holdup in the riser (ε_r)

On the basis of the literatures and previous studies, it follows that the gas holdup in the riser (ε_r) is a function of geometrical and operational variables of airlifters, Table 2.1 summarizes prediction equation of gas holdup.

Based on the evidence that, the liquid upflow in the riser of EL-ALR is similar to concurrent liquid flow in bubble columns, Hills (1976) developed equations which could be applied to airlift reactors. For $U_{L,r}$>0.3 *m/s* in air-water system, the equation can be used to calculate riser gas holdup (ε_r) for any given gas velocity under certain value of liquid velocity.

Gavrilescu and Tudose(1998) proposed an equation that can predict the gas holdup with a maximum error less than ±20%, giving satisfactory results for a relatively wide range of physical and geometrical parameters for the non-Newtonian liquids. He also experimentally compared other's work with his own, found that Popovic and Robinson's model (1984; 1988) had generally good agreement with his experimental data, with a maximum error of 23% for homogenous flow. On the contrary, Chisti's (1989) prediction equation was shown to be very scattered, the maximum error being up to 60%.

Although the forms of prediction equations varied from each others, there are generally two types of equations. One is based on empirical correlation (Bello et al. 1985; Chisti et al. 1987; Gavrilescu and Tudose 1998; Popovic and Robinson 1984; Popovic and Robinson 1988), which possesses the advantage

of easy derivation, but can only be applied to a certain style of bioreactors with similar structures. Another is well-known drift-flux model (Di Felice 2005; Freitas et al. 2000; Hills 1976) proposed by Zuber and Findlay (1965), which is independent of geometrical restrictions, but more efforts are needed on experimentally determining parameters.

Table 2.1 Summary of gas holdup studies

Reference	Experimental conditions	Model/correlation proposed
(Hills 1976)	air-water system $U_{L,r}$>0.3 *m/s*	$\varepsilon_r = \dfrac{U_{G,r}}{0.24+1.35(U_{G,r}+U_{L,r})^{0.93}}$
(Popovic and Robinson 1984)	Non-Newtonian carboxymethl cellulose d_r=0.152m A_d/A_r=0, 0.11, 0.25, 0.44 μ_{ap} =0.015 to 0.5 *Pa s* $U_{G,r}$ not specified, for bubble flow NOTE: the gas velocity in this equation is in cm/s.	$\varepsilon_r = 0.02U_{G,r}^{\,0.6504}\left[1+\dfrac{A_d}{A_r}\right]^{-1.0516}\mu_{ap}^{\,-0.1039}$ μ_{ap} based on shear rates and calculated using: $\dot{\gamma} = 5000U_{G,r}$, which is due to Nishikawa et al., (1997).
(Bello et al. 1985)	air-water d_r=0.152mr 0.0137to≤$U_{G,r}$≤0.086m/s (bubble flow only) A_d/A_r = 0.11 ~ 0.69	$\varepsilon_r = 0.16\left[\dfrac{U_{G,r}}{U_{L,r}}\right]^{0.56}\left[1+\dfrac{A_d}{A_r}\right]$ $\varepsilon_r = 3.4\times10^{-3}\left[1+\dfrac{A_d}{A_r}\right]^{-1}(P_G/V_D)^{2/3}$
(Chisti et al. 1987)	air-water 0.026≤$U_{G,r}$≤0.21m/s d_r=0.152m A_d/A_r=0.25 or 0.44 52holes Sparger, d_0=1mm.	$\varepsilon_r = 0.65\left[1+\dfrac{A_d}{A_r}\right]^{-0.258}U_{Gr}^{\,0.603+0.078C_s}$ C_s, is concentration of solids (dry wt./vol.%, g/100ml)

(Bentifraouine et al. 1997b)	Air-water $0 \le U_{G,r} \le 0.06$m/s d_r=0.194m A_d/A_r=0.48 64 holes sparger, d_0=0.8mm.	$\varepsilon_r = 2U_{G,r}^{0.88}(1-0.97U_{L,r}^{0.49})$
(Gavrilescu and Tudose 1998)	non-Newtonian liquids $1.189 \times 10^{-3}\ m^3 < V_L < 1.880 \times 10^{-3}\ m^3$ $1.16 < h_L < 1.56\ m$ h_D=1.10 m $0.111 < A_d/A_r < 0.48$ porous plate sparger	$\varepsilon_r = 4.386\left(\frac{U_{G,r}}{U_{L,r}}\right)^{0.82}\left(\frac{A_d}{A_r}\right)^{0.21}\left(\frac{h_d}{d_r}\right)^{-1} Fr^{0.164} Mo^{-0.051}$ $Fr = \frac{(U_{G,r}+U_{L,r})^2}{g \cdot d_r}$ $Mo = \frac{g(\rho_L-\rho_G)}{\sigma_L^{\ 3}\rho_L^{\ 2}} K^4 \left(\frac{8U_{L,r}}{d_r}\right)^{4(n-1)}\left(\frac{3n+1}{4n}\right)^{4n}$ K and n are power-law parameters for $\tau = K\dot{\gamma}^n$
(Freitas et al. 2000)	d_d=0.05m d_r=0.158m with 2.07m of height (H_r). The height and the diameter of top section (H_t) are 0.36m and 0.158m, respectively With a concentration that connects to a bend ($A_{t,d}$) with 0.107m diameter.	$\varepsilon_r = \frac{U_{G,r}}{C(U_{G,r}+U_{L,r})+U_{bt}}$ modification of Zuber and Findlay model 1. Orifice's diameter=0.5mm, distributing factor C=2.91, the terminal rise velocity of a single bubble U_{bt}=-0.99 2. Orifice's diameter=1.0mm, distributing factor C=2.04, the terminal rise velocity of a single bubble U_{bt}=-0.06 3. Orifice's diameter=1.6mm, distributing factor C=1.82, the terminal rise velocity of a single bubble U_{bt}=0.22
(Di Felice 2005)	$d_r = 0.05m$ $d_d = 0.10m$ Tube height can be adjusted to 1m or 2m	$\varepsilon_r = \frac{U_{G,r}}{0.25+1.1(U_{G,r}+U_{L,r})^{0.93}}$

2.1.2 Variables on gas holdup

Firstly, from above equations listed in Table 2.1, it is obvious that superficial gas velocity ($U_{G,r}$) in the riser is one of the major variables affecting gas holdup most, Since the difference in gas holdup between the riser and downcomer is the only driving force for liquid circulation in the airlift system. It is also

interesting to note that among the empirical equations, the exponent of superficial gas velocity approximately ranges from 0.6 to 0.8.

Secondly, Influence of liquid velocity ($U_{L,\ r}$) on gas holdup is also remarkable. Increased liquid circulation in the airlift may have reduced riser gas holdup because the liquid velocity was superimposed on the bubble rise velocity which, therefore, must have increased relative to that in the absence of liquid flow (Chisti 1989). Overall liquid circulation in bioreactors therefore can reduce the gas holdup in the riser of airlift reactor. This explanation can be also borrowed to understand why gas holdup in the bubble column is higher than that in EL-ALR. Because in the riser of EL-ALR, liquid velocity is one to two orders of magnitude higher than that encountered in bubble columns (Joshi et al. 1990).

Chisti (1989) reported that the increase in the riser gas holdup with declining downcomer-to-riser area ratio resulted from the reduced liquid circulation. Al-Masry and Abasaeed (1998) confirmed that, within the range they studied, increasing the A_d/A_r increased the liquid circulation velocity, shortened the time the bubbles spend in the riser thus decreases the gas hold-up in the riser.

Researchers also reported effects of unaerated liquid height (h_L) on gas holdup (Bentifraouine et al. 1997a; Chisti 1989). Chisti (1989) reported an increase of gas holdup with increasing unaerated liquid height (h_L). This is

because increased liquid height will elongate the gas retention time in the riser, unfortunately, a high gas holdup can not ensure a high mass transfer rate if the gas is depleted in oxygen during the raising process.

In Al-Masry's study (2004), the volume ratio of the liquid in the gas separator to the EL-ALR volume was found to affect the downcomer gas holdup (ε_d) for both air-water and air-glycerol systems. The author suggested that the volume ratio should be taken into consideration as a design parameter, particularly when gas recirculation into the downcomer needs to be minimized. A critical optimum volume ratio was found to be 30% for operation of the EL-ALR with the least gas entrainment in the downcomer. It is proposed that by adjusting the volume ratio, one can establish the suitable conditions for the implementation of a required chemical or biochemical process, with respect to gas hold in the downcomer.

In order to broaden the application of airlift reactors, many researchers investigated the effects of adding the solid and non-Newtonian media into the system (Popovic and Robinson, 1984; Chisti et al., 1986; Popovic and Robinson, 1989; Gavrilescu, 1998). It was conclude by Petersen and Margaritis (2001) that, for low-density particles (e.g., activated carbon) gas hold-up is relatively unaffected by particle size, solids loading, however, for heavier particles, (e.g. glass beads or bronze particles), the overall gas hold-up decreases in solids loading.

2.1.3 Gas holdup measurements

A common method to estimate the overall gas holdup is to measure the distance between ungassed and gassed liquid level. (Petersen and Margaritis 2001). Chisti et al. (1989) suggested that overall gas holdup can be measured by using volume expansion technique by using following equation:

$$\varepsilon = \frac{h_D - h_L}{h_D} \qquad (2.1)$$

where h_D is the dispersion height of gas-liquid mixture; h_L is unaerated liquid height. The gas holdup predicted by using Eq. 2.1 was reproducible within ±10% even at the highest gas flows (~0.21*m/s*) (Chisti 1989).

Differing from overall gas holdup, local gas holdup indicates the individual gas containing within a certain section in the riser or in the downcomer. The most common method to measure local gas holdup uses a series of manometric pressure tap placed throughout the bioreactor and measures the pressure drop along the flow path.

The manometric technique can be applied to measure the individual, local gas holdups in the riser and the downcomer by using following equation:

$$\varepsilon_{r(d)} = 1 - \frac{\Delta P}{\rho_L g \Delta h} \qquad (2.2)$$

where ΔP and Δh represent pressure drop and distance between two ports of pressure taps.

Merchuk et al. (1996) pointed out that the location of the pressure tap is

very important especially when measuring pressure drops in small lab-scale airlift bioreactor. It was suggested that, the flow must be completely developed before the measuring point in order to ensure the static pressure with no interference from the dynamics of the fluid.

2.2 Liquid Circulation Velocity $U_{L,r(d)}$

Liquid circulation velocity in air-lifter is a crucial operational variable that can greatly affect the performance of bioreactors, such as mixing time (Merchuk et al. 1996), oxygen mass transfer (Sotiriadis et al. 2005), downcomer gas holdup (Chisti 1989), flow regime transition (Bendjaballah et al. 1999), and adhesive strength of biofilms (Chen et al. 2005).

There are two types of equations that have been widely used to predict the liquid velocity of airlift bioreactors. One is empirical equation, it has the advantage of easy derivation but can be only applied to a certain type of bioreactors (Al-Masry and Abasaeed 1998; Bello et al. 1984; Glennon et al. 1993; Popovic and Robinson 1984; 1988). Another is semi-empirical equation which is based either on analysis of energy or momentum balance throughout the flow path inside airlift bioreactors(Chisti 1989; Di Felice 2005; Freitas et al. 2000).

After further comparison, the equations and models, which are derived from momentum balance or based on local pressure analysis, are actually based on

the same theory of energy balance, as summarized in table 2.2. For incompressible, steady fluid flow investigated in most of industrial cases, the amount of energy (E, *W*) consumed in each part of a reactor can be estimated as the product of pressure difference (ΔP, *Pa*) and volumetric flow rate (Q, m^3/s) as follows:

$$E=\Delta P \cdot Q \qquad (2.3)$$

Table 2.2 Summary of prediction equation of liquid circulation velocity

Reference	Experimental conditions	Model/correlation proposed
(Kawagoe and Robinson 1980)	air-water $U_{G,r}$<0.03m/s d_r=0.152m A_d/A_r=0.44	$U_{L,r} \propto U_{G,r}^{0.48}$
(Onken and Weiland 1980)	Air-water and Newtonian media $\mu \approx$ 1~16mPas d_r=0.1m d_d=0.05m h_D=8.5m 0.006m/s≤$U_{G,r}$≤0.16m/s	$U_{L,r} \propto U_{G,r}^{0.4}$
(Bello et al. 1984)	air-water and 0.15 kmol/m^3 NaCl, 0.5M NaCl h_D=1.8m d_r=0.152m A_d/A_r=0.11, 0.25, 0.44 0.0137m/s≤$U_{G,r}$≤0.086m/s Sparger: perforated stainless plate with 52 holes of 1.02mm	$U_{L,r} = 1.55\left[\frac{A_d}{A_r}\right]^{0.74\pm0.04} U_{G,r}^{1/3}$
(Popovic and Robinson 1984)	Non-Newtonian carboxymethl cellulose. d_r=0.152m A_d/A_r=0, 0.11, 0.25, 0.44 μ_{ap} =0.015 ~ 0.5 Pas $U_{G,r}$ was not specified, for bubble flow only NOTE: the gas velocity in this equation	$U_{L,r} = 0.052 U_{G,r}^{0.322}\left[\frac{A_d}{A_r}\right]^{0.794} \mu_{ap}^{-0.395}$ μ_{ap} based on shear rates and calculated using: $\dot{\gamma} = 5000 U_{G,r}$ which is due to Nishikawa et al., (1997)

is in cm/s.

(Popovic and Robinson 1988)	Non-Newtonian carboxymethl cellulose. d_r=0.152m A_d/A_r=0, 0.11, 0.25, 0.44 μ_{ap} =0.015 ~ 0.5 Pas U_{Gr} not specified h_D=1.88m	$U_{L,r} = 0.23 U_{G,r}^{0.32} \left[\frac{A_d}{A_r}\right]^{0.97} \mu_{ap}^{-0.39}$ μ_{ap} based on shear rates and calculated using: $\dot{\gamma} = 5000 U_{G,r}$ which is due to Nishikawa et al., (1997)
(Chisti 1989)	Air-water A_b/A_d =1 ~ 2 A_b/A_r=0.25 ~ 1.0 L_{cp}/d_{cp}=2 ~ 7	$U_{L,r} = \left[\frac{2gh_D(\varepsilon_r - \varepsilon_d)}{\frac{K_T}{(1-\varepsilon_r)^2} + K_B\left(\frac{A_r}{A_d}\right)^2 \frac{1}{(1-\varepsilon_d)^2}}\right]^{0.5}$ The model was shown to apply to several distinct types of airlifts: draught-tube internal-loop (annulus and draught-tube sparged), split-cylinder internal-loop and external-loop devices.

(Gavrilescu and Tudose 1995; 1998)	for $U_{G,r}$<0.04m/s at 21±1°C 10^5Pa ε_d =0 (1) Laboratory reactor: d_r=0.03m 1.189×10^{-3} m^3≤ Liquid volume in the bioreactor ≤$1.880\times10^{-3}m^3$ 0.016m/s≤$U_{G,r}$≤0.177m/s 0.111≤A_d/A_r≤1.000 H_d (Ungassed liquid height in downcomer)=1.0m; 1.16m≤ H_r (Ungassed liquid height in riser)≤1.56m (2) Pilot scale reactor: d_r=0.2m 0.157m^3≤ Liquid volume in the bioreactor ≤0.170m^3 0.010m/s≤$U_{G,r}$≤0.120m/s 0.04≤A_d/A_r≤0.1225 4.0m≤ H_d ≤4.4m 4.3m≤ H_r ≤4.7m	$$U_{L,r}=1.2\left(\frac{A_d}{A_r}\right)^{0.657}U_{G,r}^{0.4}$$ After experimental data collecting, by using non-linear regression, the above empirical equation was derived with a standard deviation of 0.067. (1995) $$U_{L,r}=4.25U_{G,r}^{a}\left(\frac{A_d}{A_r}\right)^{0.95}\left(\frac{H_s}{H_D}\right)^{0.3}$$ The experimental $U_{L,r}$ data obtained in both external-loop airlift bioreactors with air-water dispersions were correlated using non-linear regression in the above equations. (1998) H_s, difference between ungassed liquid height in riser and in downcomer; H_D, ungassed liquid height in downcomer. a=0.42, for $U_{G,r}$≤0.04m/s (bubble flow regime) a=0.47, for 0.04m/s<$U_{G,r}$≤0.07m/s (transition regime) a=0.54, for $U_{G,r}$>0.07m/s (heterogeneous, turbulent regime)
(Glennon et al. 1993)	Cited by Al-Masry and Abasaeed (1998)	$$U_{L,r}=1.017\Re^{-0.409}U_{G,r}^{0.420}(U_{G,r}\le 0.05m/s)$$ $$U_{L,r}=0.753\Re^{-0.427}U_{G,r}^{0.315}(U_{G,r}\ge 0.05m/s)$$ $$\Re=\frac{\Sigma K}{2gh_D}\left(\frac{A_r}{A_D}\right)^2$$
(Al-Masry and Abasaeed 1998)	d_r=0.1m or 0.23m or 0.23m 0.018m/s≤$U_{G,r}$≤0.124m/s A_d/A_r= 0.25 or 0.44 or 1.0 No gas recirculation. A plate sparger had 1mm perforations.	$$U_{L,r}=\alpha\left(\frac{\rho_L U_{G,r}h_D}{\mu_L}\right)^{\beta}\left(\frac{1}{1+A_d/A_r}\right)^{\delta}\left(\frac{V_{separator}}{V_{working}}\right)^{\gamma}$$ $V_{separator}$ is the volume of the gas-liquid separator. $V_{working}$ is the working volume of the liquid. α =0.95 β =0.165 δ =1.84 γ =1.38

(Freitas et al. 2000)

d_d =0.05m

d_r =0.158m ith 2.07m of height (H_r).

The height and the diameter of top section (H_t) are 0.36m and 0.158m, respectively

With a concentration that connects to a bend ($A_{t,d}$) with 0.107m diameter.

1. Orifice's diameter=0.5mm, β =0.0095
2. Orifice's diameter=1.0mm, the parameter β =0.0044
3. Orifice's diameter=1.6mm, the parameter β =0.0069

$$2gH\varepsilon_r = \left[\frac{(H_r + H_t)d_r^{-1.25}}{(1-\varepsilon_r)^{1.75}} + \left(\frac{A_r}{A_d}\right)^{1.75}(H_d + H_b)d_d^{-1.25}\right]\cdot \beta U_{L,r}^{1.75} + k_{fr,t}\frac{U_{L,r}^2}{(1-\varepsilon_r)^2} + \left[\left(\frac{A_r}{A_{t,d}}\right)^2(k_{ft,d} + k_{fge}) + \left(\frac{A_r}{A_d}\right)^2(k_{fse} + K_{fd,b} + k_{fb,r})\right]U_{L,r}^2$$

$K_{ft,d}$, $K_{fd,b}$, $K_{fr,t}$ and $K_{fb,r}$ are the fitting friction coefficients.

K_{fge} and K_{fse} are the friction coefficients due to diameter change

(Di Felice 2005)

$d_r = 0.05m$

$d_d = 0.10m$

Tube length can be adjusted to 1m or 2m

driving force:

$$\Delta P = H\rho_L \varepsilon g = \Delta P_e + \Delta P_D$$

Friction pressure loss:

$$\Delta P_D = \frac{1}{2}H\rho_L\left(\frac{f_r}{d_r}U_{L,r}^2 + \frac{f_d}{d_d}U_{L,d}^2\right)$$

$$f_r = \frac{0.316}{\mathrm{Re}^{0.25}} = \frac{0.316}{(Q_L\rho_L / d_r\mu_L)^{0.25}}$$

$$f_d = \frac{0.316}{\mathrm{Re}^{0.25}} = \frac{0.316}{(Q_L\rho_L / d_d\mu_L)^{0.25}}$$

Concentrated pressure losses:

$$\Delta P_e = \frac{1}{2}K_r\rho_L U_{L,r}^2 + \frac{1}{2}K_d\rho_L U_{L,d}^2$$

K_r and K_d may be estimated from fig. 8.15 of R.W.Fox (1998)

2.2.1 Prediction equation based on energy balance

Among all these researchers, Chisti (1989) proposed a general model for predicting liquid circulation velocity based on energy balance. The model could

be applied to several types of airlifters: draught-tube internal-loop, split-cylinder internal-loop and external-loop airlift bioreactors.

In this study, air-water mixture is treated as impressible fluid*, therefore, density of air-water mixture can be reasonably calculated based on air and water densities under the same conditions. On the basis of energy balance, according to Chisti (1989)'s summary, it gives:

Rate of energy input into reactor = Rate of energy dissipation,

which can be further expressed as

$$E_i = E_r + E_d + E_b + E_t + E_{fr} + E_{fd} \qquad (2.4)$$

E_i = energy input due to isothermal gas expansion and kinetic energy of air

$$= QP_h \ln\left(1 + \frac{\rho_D g h_D}{P_h}\right) \qquad (2.5)$$

E_r = energy dissipation due to wakes behind bubbles in the riser.

E_d = energy loss due to stagnant gas swarm in the downcomer.

$E_b + E_t$ = energy loss due to sudden expansion and contraction at the bottom and top of reactor.

$E_{fr(fd)}$ = energy loss to friction in the riser (downcomer).

Energy balance in the riser

Using the liquid in the riser as the control volume, Chisti (1989) analyzed individual riser in airlift bioreactors based on mechanical-energy-balance (as

* Sound's velocity in air is v=340m/s, in water is c=1435 m/s (1.8°C), Mach number equals to v/c, when v/c<<1, the fluid can be treated as incompressible.

shown in Fig. 2.1):

$$\frac{1}{2}\left(v_2^2 - v_1^2\right) + g\left(z_2 - z_1\right) + \frac{p_2 - p_1}{\rho_L} + \sum F + W_s = 0 \qquad (2.6)$$

where W_s is the work done by the liquid; $\sum F$ is the sum of energy losses per unit mass; $v_{1(2)}^2/2$, $zg_{1(2)}$, and $p_{1(2)}/\rho_L$ are the kinetic energy, potential energy and static pressure of point 1 and 2, respectively. Compared to energy dissipation due to the wakes, frictional energy loss was reasonably ignored in conventional airlift bioreactors (Chisti 1989). Therefore, in the following process of derivation, the term of frictional energy loss included in $\sum F$, is ignored.

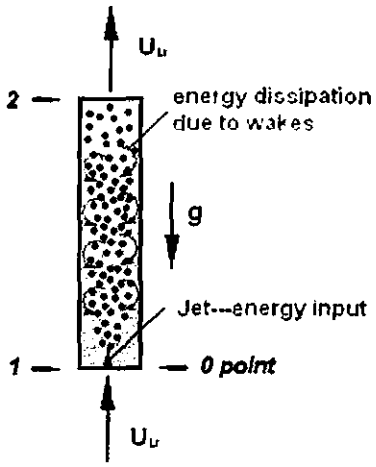

Fig. 2.1. Schematic diagram of liquid upflow in the riser

Based on Eq. 2.6, in the riser of an EL-ALR, energy dissipation due to the wakes behind the bubbles can be obtained by applying mechanical-energy balance on the control volume of riser liquid. Thus,

$$E_i = E_r - \rho_L g h_D (1-\varepsilon) U_{L,r} A_r + \rho_L g h_D U_{L,r} A_r \qquad (2.7)$$

On the right-hand side of Eq. 2.7, the second and the third term are *pressure energy loss* and *potential energy gain* along with the liquid upflow in the riser, respectively. After rearranging,

$$E_r = E_i - \rho_L g h_D U_{L,r} A_r \varepsilon \qquad (2.8)$$

Energy balance in the downcomer

Similarly, energy loss arising from the drag of gas bubbles (Fig 2.2) on liquid in the downcomer is obtained by performing a mechanical energy balance in the downcomer, using the downcomer liquid as the control volume (Chisti 1989):

$$0 = E_d + \rho_L g h_D (1-\varepsilon_d) U_{L,d} A_d - \rho_L g h_D U_{L,d} A_d \qquad (2.9)$$

On the right-hand side of Eq. 2.9, the second and the third term represent *pressure energy gain* and *potential energy loss* along with the liquid downflow in the downcomer, respectively. After rearranging, it gives

$$E_d = \rho_L g h_D U_{L,d} A_d \varepsilon_d \qquad (2.10)$$

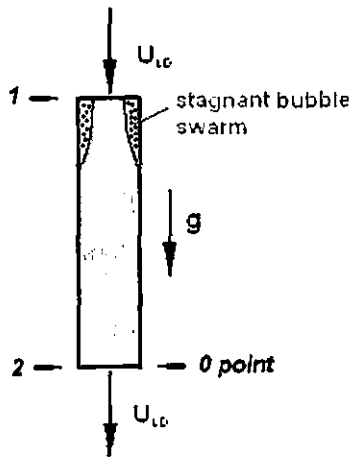

Fig. 2.2. Schematic diagram of liquid downflow in the downcomer

Energy losses in the top and the bottom sections

Chisti (1989) proposed that the energy losses in the top and the bottom sections of an airlift bioreactor can be calculated in exactly the same way as for pipe flow. Thus,

$$E_t + E_b = \frac{1}{2}\rho_L\left[V_{L,r}^3 K_T A_r(1-\varepsilon_r) + V_{L,d}^3 K_B A_d(1-\varepsilon_d)\right] \qquad (2.11)$$

where K_T and K_B are the friction loss coefficient for the top and the bottom connecting sections, respectively. $V_{L,r}$ and $V_{L,d}$ in Eq. 2.11 are the true linear liquid velocities or the interstitial velocities in the riser and the downcomer, respectively, and are related to the corresponding superficial liquid velocities in the following manner:

$$V_{L,r} = \frac{U_{L,r}}{1-\varepsilon_r} \qquad (2.12)$$

and $$V_{L,d} = \frac{U_{L,d}}{1-\varepsilon_d} \qquad (2.13)$$

Furthermore, the continuity equation can be employed to convert riser and downcomer superficial liquid velocities to each other:

$$A_r \cdot U_{L,r} = A_d \cdot U_{L,d} \qquad (2.14)$$

Finally, by substituting Eq. 2.8, 2.10 and 2.11 into Eq. 2.4, the liquid circulation velocity in the riser of an airlift bioreactor can be expressed as the following form;

$$U_{L,r}=\left[\frac{2gh_D(\varepsilon_r-\varepsilon_d)}{\frac{K_T}{(1-\varepsilon_r)^2}+K_B\left(\frac{A_r}{A_d}\right)^2\frac{1}{(1-\varepsilon_d)^2}}\right]^{0.5} \qquad (2.15)$$

Differing from the work proposed by Chisti (1989), Gavrilescu and Tudose (1995) suggested a simple, general model to correlate liquid velocity directly with superficial gas velocity as follows:

$$U_{L,r}=aU_{G,r}{}^{b} \qquad (2.16)$$

values of *a* and *b* might not remain constant for the entire range of gas input therefore should be experimentally determined for lab and pilot scale reactors, respectively. After experimental data collecting, by using non-linear regression, Gavrilescu and Tudose (1995) derived the following empirical equation according to Eq. 2.16 (For $U_{G,r}$<0.04m/s, with a standard deviation of 0.067):

$$U_{L,r}=1.2\left(\frac{A_d}{A_r}\right)^{0.657}U_{G,r}{}^{0.4} \qquad (2.17)$$

Although there are existing different ways to derive the prediction model, the essential task of modeling liquid circulation velocity is to find the relationship between drive force and over all friction loss.

As we already summarized in Table 2.2, different researchers investigated airlift reactors based on different configurations. Therefore, actually, each model based on experimental data can only be applied to the reactors with exactly similar geometry, which in turn restrict its application within a relative

small range. For example, empirically derived equations (Glennon et al. 1993) were evaluated by Al-Masry and Abasaeed (1998) and were found that the equations provided good predictions for the small and medium reactors but worsened when compared to experimental data from large reactor.

On the contrary, prediction equations based on energy or momentum balance is aimed to solve the problem from basic physical phenomena-two phase flow, and their derivative procedures are theoretically solid. As proposed by Joshi et al. (1990), such models and equations constituted a set of non-linear equations for the estimation of liquid velocity, involving an iterative procedure. Based on Joshi and his coworker's original concepts, Camarasa et al. (2001a) developed a complete model for external-loop airlift reactors, they divided the airlifting system into three sections, and solved a series of equations by combining the energy balance and the momentum balance with respect to different sections of the bioreactor.

2.2.2 Effects on liquid circulation velocity

In airlift bioreactors, gas sparing is the only source providing energy for overall liquid circulation. Therefore, it is obvious that the circulation liquid velocity increases with increasing the superficial gas velocity ($U_{G,r}$) (Choi 2002).

Compared with the internal-loop, draught-tube airlifters in which the

entrainment of small bubbles in the downcomer was higher, Bello et al. (1984) found that higher circulation velocities were obtained on the external-loop airlift bioreactors where there was relatively low downcomer gas holdup.

Gavrilescu and Tudose (1995) reported that geometric parameter A_d/A_r influenced the overall friction, resulting in changes of liquid velocity. At a given gas superficial velocity and riser cross-sectional area, increasing the downcomer area (A_d) would lower the resistance of flow in the downcomer, which in turn would tend to increase the liquid circulation velocity if under the same hydrodynamic driving force.

Choi (2002) systematically investigated the effects of the unaerated liquid height (0~0.2m), the superficial gas velocity (0.02~0.18m/s) and the downcomer-to-riser cross-sectional area ratio (0.11~0.53) on the hydrodynamic characteristics in EL-ALR. It was found that as the unaerated liquid height increased, the circulation liquid velocity increased due to an increase in the density difference between the dispersion phases in the riser and the downcomer.

2.2.3 Measurement of liquid circulation velocity

Chisti (1989) employed a tracer method to measure liquid circulation in airlift bioreactors. Concentrated sulfuric acid (~8M) was used as a tracer. It was poured (typical volume=0.2~0.4L) instantaneously into the top of the

downcomer and the pH was followed at two downstream locations by identical pH electrodes placed some distance ($d_{electrode}$) apart in the downcomer. From the measured time interval between the tracer peaks (t_{peaks}) from the two pH electrodes and the known vertical distance between them, the linear liquid velocity in the downcomer could be calculated by using the following equation:

$$V_{L,d} = \frac{d_{electrode}}{t_{peaks}} \qquad (2.18)$$

In Camarasa et al.'s work (2001b), the circulation velocity of the liquid phase was measured with an ultrasonic transit-time flowmeter (Controlotron®, System 1010P UNIFLOW) located in the downcomer.

Generally speaking, ultrasound techniques allow instantaneous measurement of only one characteristic of the dispersed phase at a time; furthermore, they are ineffective under high gas holdup conditions (more than 20%), because the acoustic signal is lost due to repeated reflections (Boyer et al. 2002).

As suggested by Boyer an shi coworkers(2002), pressure measurement is a robust and easy way of flow diagnosis. Though wall pressure transducers are widely applied nowadays, but intrusive pressure probes, so-called Pitot tubes, are still very useful. Pitot tubes can be applied to hostile environments (when gas–liquid flow includes solid particles). Nicol and Davidson (1988) estimated the error made on liquid-phase mean velocity measurement to some

4%.

2.3. Oxygen mass transfer (k_La)

Oxygen is one of the most important substrates in aerobic fermentation. It is a factor which influences the direction of aerobic metabolism of microbial cells. In aerobic fermentation, it is very important to increase the oxygen transfer rate to the fermentation media because oxygen can be regarded as a nutrient for aerobic microorganisms. Growing microorganisms are capable of metabolizing oxygen from the liquid faster than it can be supplied. The solubility of oxygen in liquid media is quite low, while its demand for the growth is high. If oxygen supply drops too low, the system may become anaerobic (Hensirisak 1997).

During fermentation, the transfer of oxygen from an air bubble to the cell can be represented by a number of steps. The sparingly oxygen is transferred from a rising gas bubble into a liquid phase and ultimately to the site of oxygen reaction in a cell particle.

In pneumatically agitated bioreactor, the transport of oxygen from gas phase to liquid phase is controlled by the liquid-phase mass transfer coefficient, k_L. To determine the total oxygen transfer rate in a fermentor, the total surface area available for mass transfer, a, has to be know. Separate determination of k_L and a is difficult to evaluate and sometime impossible. The combine term of k_La is usually reported as the mass transfer coefficient rather than just k_L

(Doran 1995).

Previous studies and researches on oxygen mass transfer in airlift bioreactors have been collected and summarized in Table 2.3

Table 2.3 Summary of prediction equation of oxygen mass transfer (k_La)

Reference	Experimental conditions	Model/correlation proposed
(Popovic and Robinson 1984)	Non-Newtonian carboxymethl cellulose. d_t=0.152m A_d/A_r=0, 0.11, 0.25, 0.44 μ_{ap} =0.015 to 0.5 Pas $U_{G,r}$ not specified, for bubble flow NOTE: the gas velocity in this equation is in cm/s.	$k_La = 1.911\times10^{-4}U_{G,r}^{0.525}\left[1+\frac{A_d}{A_r}\right]^{-0.853}\mu_{ap}^{-0.89}$ μ_{ap} based on shear rates and calculated using: $\dot{\gamma} = 5000U_{G,r}$, which is due to Nishikawa et al., 1977.
(Bello et al. 1985; 1985a)	air-water d_t=0.152m 0.0137to≤$U_{G,r}$≤0.086m/s (bubble flow only) A_d/A_r = 0.11 ~ 0.69	1985 $\frac{k_La_Dh_D}{U_L} = 2.28\left[\frac{U_{G,r}}{U_L}\right]^{0.90}\left[1+\frac{A_d}{A_r}\right]^{-1}$ 1985a: $k_La_D = 0.76\left[1+\frac{A_d}{A_r}\right]^{-2}U_{G,r}^{0.8}$ $k_La_D = 5.5\times10^{-4}\left[1+\frac{A_d}{A_r}\right]^{-1.2}(P_G/V_D)^{0.8}$ Where $a_D = a_L/(1-\varepsilon_r)$
(Chisti 1989)	air-water 0.026≤$U_{G,r}$≤0.21m/s d_t=0.152m A_d/A_r=0.25 or 0.44 52holes Sparger, d_0=0.001m.	$k_La = \left[1+\frac{A_d}{A_r}\right]^{-1}(0.349-0.102C_s)U_{G,r}^{0.837\pm0.62}$ C_s, is concentration of solids (dry wt./vol.%, g/100ml)

(Al-Masry and Abasaeed 1998)	air-water d_r=0.1m or 0.23m or 0.23m 0.018m/s≤U_{Gr}≤0.124m/s A_d/A_r= 0.25 or 0.44 or 1.0 No gas recirculation. A plate sparger had 1mm perforations.	$k_L a = \alpha\left(\frac{\rho_L U_{Gr} h_D}{\mu_L}\right)^{\beta}\left(\frac{1}{1+A_d/A_r}\right)^{\delta}\left(\frac{V_{separator}}{V_{working}}\right)^{\gamma}$ $V_{separator}$ is the volume of the gas-liquid separator. $V_{working}$ is the working volume of the liquid. α =0.484 β=0.76 δ=-2.41 γ=1.9

2.3.1 Effects on oxygen mass transfer

Benyahia and Jones(1997) investigated oxygen transfer in two geometrically similar EL-ALR with linear scale ratio of 2. In mass transfer experiments, the sampling location was found to be important as significantly different k_La values were obtained. The variations of k_La with probe location have been explained in terms of non-uniform hydrodynamic properties. By using high speed video camera, authors reported that at higher gas flow rates, the gas hold-up was significantly higher in the large-scale reactor. It was found that in order to maintain the gas hold-up or k_La constant in both the small- and large-scale reactor, the small-scale reactor required 25% and 27% more power input per unit volume of liquid respectively.

Rubio et al. (2001) investigated the axial profiles of dissolved oxygen concentration in tall airlift reactors, which were frequently ignored. It was found that following reactor geometry parameters affect the oxygen concentration profiles: the static height of liquid in the vessel, the cross-sectional areas of the riser and the downcomer channels, and the cross-sectional area available for

flow under the baffle or the draft-tube.

Oxygen mass transfer in a forced circulation pumped loop reactor was investigated by Fadavi and Chisti (2005). It was found that higher values of forced circulation rate reduced mass transfer efficiency, but reactor was always more efficient than a propeller loop reactor. More and small bubbles were observed, compared to operation as an airlift reactor.

In Nikakhtari and Hill's work (2005), a stainless steel mesh packing with 99.0% porosity was inserted in the riser section of an EL-ALR to compare the oxygen mass transfer rates both with and without packing. It was reported that the packing increased the overall volumetric oxygen mass transfer coefficient by an average factor of 2.45 compared to the unpacked column. The packing increased gas holdup, decreased bubble size, and decreased liquid circulation rates in the bioreactor, all of which contributed to the dramatic improvement in the oxygen mass transfer rates.

In addition to geometric and operational effects as discussed above, influences of properties of liquid on oxygen mass transfer coefficient has also been widely investigated. Kawase and Hashimoto (1996) studied the effects of solids loading on gas hold-up and oxygen transfer in external-loop airlift bioreactors with non-Newtonian fermentation media. Experiments were performed in two EL-ALRs with aqueous solutions of carboxymethyl cellulose (CMC) and xanthan gum representing non-Newtonian flows. It was found that

the extent of effects of solid contains on oxygen mass transer depended on non-Newtonian flow behavior, for the inelastic non-Newtonian CMC aqueous solutions, the presence of low-density solid particles slightly increased the riser gas hold-up (ε_r), but decreased the volumetric mass transfer coefficient (k_La). On the other hand, ε_r decreased but k_La increased with solids loading in the viscoelastic non-Newtonian xanthan gum aqueous solution.

2.3.2 Measurement of oxygen mass transfer

Dynamic method, which is based on an unsteady-state mass balance for oxygen, has been widely used to measure the oxygen mass transfer (Chisti 1989; 1987; Fadavi and Chisti 2005). The main advantage of the dynamic method over steady-state technique is the low cost of the equipment (Doran 1995).

By applying dynamic method, initially, the airlift bioreactors contained tap water in batch. At some time t_0, the liquid inside ALR was de-oxygenated by sparging nitrogen into the vessel. Dissolved oxygen concentration drops during this period. Air is then pumped into the broth at a constant flow rate and the increase in dissolved oxygen concentration monitored as a function of time. During the re-oxygenation step, the system is not at steady state. The rate of change in dissolved-oxygen concentration during this period is equal to the rate of oxygen transfer from gas to liquid, ignoring the rate of oxygen uptake by

aerobic microorganisms (Doran 1995).

Chapter 3. MATERIALS AND METHODS

3.1 Reactor configuration

Fig.3.1 is a schematic diagram of the multiple airlifting membrane bioreactor (MAMBR) made from acrylic plastics. The vessel had a diameter of 0.28 m and an overall height of 1.10 m. Four sintered stainless steel filter tubes (GKN Sinter Metals, IL, U.S.A.) were installed between the bottom (0.088 m) and top (0.25 m) sections, separating the vessel into two compartments, a tube-side aerobic compartment of 0.016 m^3 and a shell-side anaerobic compartment of 0.032 m^3.

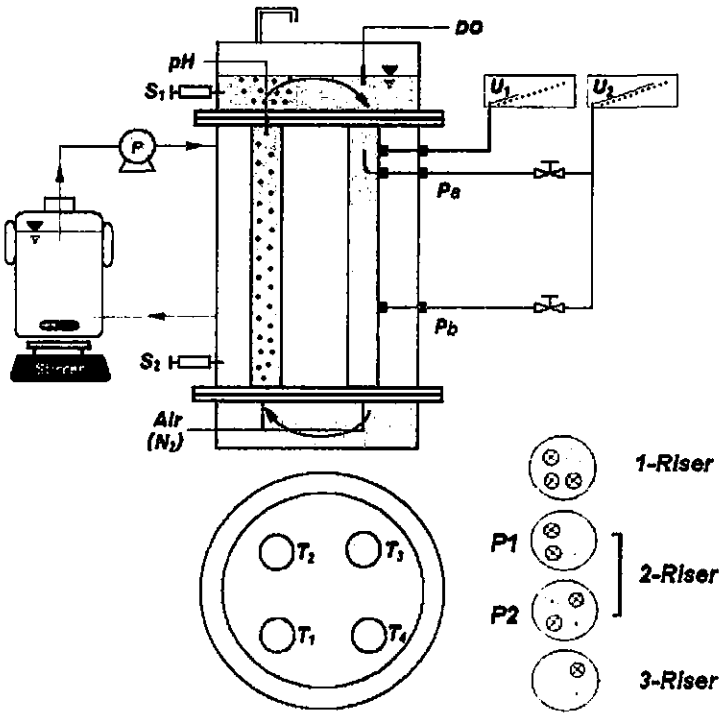

Fig.3.1. Schematic diagram of the multi-airlifting membrane bioreactor (MAMBR). Symbles: Air (N_2), inlets of air or nitrogen gas; DO, dissolved oxygen probe; pH, pH probe; P_a and P_b,

ports of pressure measurement; T1~T4, stainless steel membrane tube; U1and U2, inclined manometer for pressure measurement; S1and S2, liquid sampling ports.

Air and water were the working media for the study, and all the experiments were conducted at 23±1°C. Air could be sparged into the individual tubes (risers) at the bottom through a jet (orifice diameter of 1 mm). Air bubbles rose up in the risers and left water in the top degassing section. The degassed water flowed into the tubes that were not aerated (downcomers) forming overall liquid circulations as shown in Fig. 3.1. Three operation modes were investigated by introducing air into one, two, and three risers, respectively, while the rest tube(s) as the downcomer(s). The number of airlifting in the MAMBR, therefore, could be easily changed for studies on hydrodynamics and mass transfer. For two risers, there were two arrangements of the risers and downcomers, a parallel pattern (P1) and a diagonal pattern (P2). The stainless steel filter tubes had an external diameter of 6.5 cm and a wall thickness of 2.5 mm with a porosity of 20 % and average pore size of 10 micron. In addition to oxygen mass transfer in the aerated tube-side compartment, molecular diffusion of substances such as nutrients and metabolic products also occurs across the porous walls of the filter tubes under concentration gradients. This novel multiple airlifting membrane bioreactor, therefore, could efficiently integrate aerobic and anaerobic cultures or fermentations in one single vessel.

3.2 Experimental measurements

3.2.1 Gas holdup and liquid velocity.

The air flow rate in individual risers was controlled and measured with a needle valve and flow meter (Cole-Parmer, IL, U.S.A.). In order to measure the liquid velocity and gas hold up in the risers and downcomers, one stainless steal filter tube was replaced with a transparent acrylic tube of the same size as shown in Fig. 3.2.

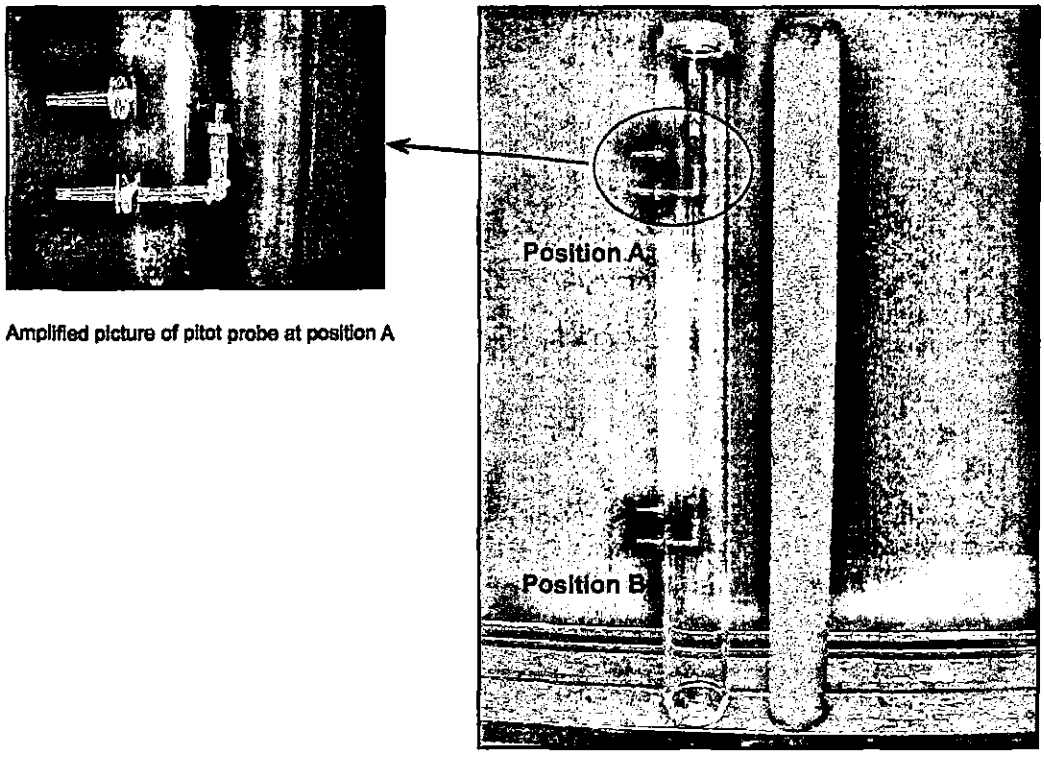

Amplified picture of pitot probe at position A

Fig. 3.2. Pictures of Acrylic tube and porous tube

Without aeration, the tube performed as a downcomer, and according to

the working principal of a Pitot tube, the liquid velocity at the tube center was measured as press drop against the wall. For turbulent pipe flow, the average velocity is about 80% of the maximum velocity measured (Geankoplis 2004). Two inclined manometers were used to measure the pressure difference.

In the amplified picture (Fig. 3.2) at position A, the pertinent parameters used in Bernoulli equation are defined below,

Point 1 (static pressure point): height z_1, pressure p_1, liquid velocity v_1

Point 2 (static + velocity pressure): height z_2, pressure p_2, liquid velocity v_2

The pressure drop can be calculated from the difference of liquid levels between two inclined U-tubes. Write the Bernoulli equation between point 1 where the velocity v_1 is undisturbed before the fluid decelerates, and point 2, where the velocity v_2 is regarded as zero:

$$z_1 + \frac{v_1^2}{2g} + \frac{p_1}{\gamma} = z_2 + \frac{v_2^2}{2g} + \frac{p_2}{\gamma} \qquad (3.1)$$

Setting $v_2 = 0$ and solving for v_1,

Substituting $\gamma = \rho_L g$, $z_1 = z_2$, into Eq. 3.1, gives,

$$v_1 = \sqrt{\frac{2 \cdot (p_2 - p_1)}{\rho_L}} = U_{L,d} \qquad (3.2)$$

where $U_{L,d}$ represents superficial liquid velocity in the testing tube (downcomer of MAMBR).

With aeration, the tube performed as a riser. The fluid density difference

between two ports (P_a and P_b, ΔH = 38.1cm apart) was measured and converted to gas holdup in the riser. The gas holdup of individual risers (ε_r) or downcomers (ε_d) is determined with Eq. 3.3*.

$$\varepsilon_{r(d)} = \frac{\Delta h}{\Delta H}, \qquad (3.3)$$

where Δh is the pressure difference between the two ports. An overall gas holdup (ε_v) based on total aerobic volume of tube-side compartment is estimated with Eq. 3.4.

$$\varepsilon_v = \frac{m \cdot \varepsilon_r \cdot V_t}{m \cdot \varepsilon_r \cdot V_t + V_L}, \qquad (3.4)$$

where m is the number of risers, and V_t and V_L are the volume of individual tube and liquid volume of tube-side compartment, respectively.

3.2.2 Calibration of liquid velocity measurement

For liquid velocity measurement in downcomer, a calibration facility of similar structure was used to calibrate the water flow rate with the inclined manometers (Fig. 3.3).

* See Appendix A for details

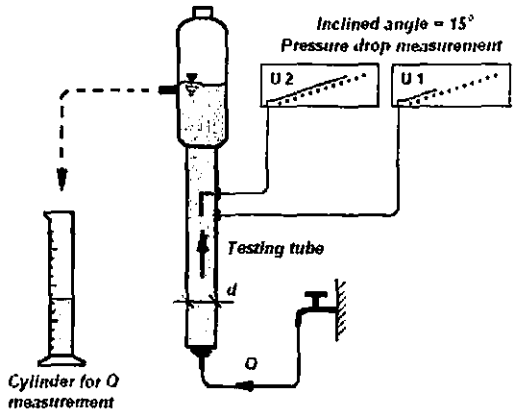

Fig.3.3 Schematic of Pitot tube calibration system

One pair of Pitot tubes was mounted on a pipe (25 *mm* inside diameter) to measure the pressure difference when tap water flew upward at different volumetric rates. Based on Bernoulli equation, the superficial liquid velocity ($U_{L,t}$) was correlated with the measured pressure drop (ΔP) (Eq. 3.5).

$$U_{L,t} = C_p \sqrt{\frac{2\Delta P}{\rho_L}} \qquad (3.5)$$

Where C_p is a dimensionless coefficient and ρ_L is the water density. At a liquid velocity ranging from 0.13 to 0.47*m/s*, the value of C_p is 0.901 as shown in Fig. 3.4, in agreement with the reported values of 0.98 to 1.0 (Geankoplis 2004)

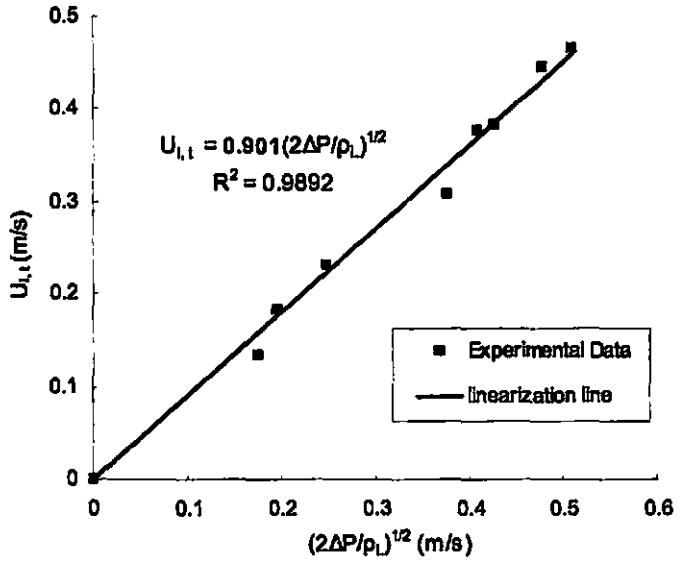

Fig.3.4 Calibration between the liquid velocity in testing tube ($U_{L,t}$) and pressure drop ($\sqrt{2\Delta P/\rho_L}$) based on Eq. 3.5.

3.2.3 Measurement of circulation time.

Acid tracer was used to measure the overall mixing time (t_m) for 95% homogeneity and liquid circulation time (t_c) for one complete cycle between riser and downcomer. Five milliliters of hydrochloric acid solution (~5M) was injected into the liquid above a downcomer, and a pH probe (model UP-10, Denver, Col., USA) located above a riser was used to monitor the change of solution pH with time (Fig.3.5). The circulation time was estimated by taking an average value of consecutively time intervals between two pH peaks (Chisti 1989).

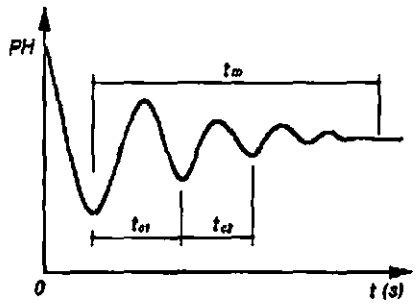

Fig.3.5 Measurement of mixing time

3.2.4 Oxygen mass transfer coefficient k_La.

The value of k_La under different operation conditions was determined by a dynamic method (Chisti 1989). A dissolved oxygen probe (BIOFLO® 110 fermentor) was mounted in the top section right above a downcomer as shown in Fig.3.1. Dissolved oxygen (DO) was first removed by sparging nitrogen gas till the DO concentration near zero. Aeration was then started with different number of risers at different superficial gas velocities and a time course was recorded till a steady state DO concentration was reached. The volumetric oxygen mass transfer coefficient k_La was estimated with Eq. 3.6.

$$\ln\frac{C^* - C_{L0}}{C^* - C_L} = k_L a \cdot t \qquad (3.6)$$

where C^*, C_{L0} and C_L are saturated, initial and instantaneous concentration of dissolved oxygen in water, respectively, and t refers the time. Let left hand side's concentration ratio of Eq.3.6 divide by C^*, yields,

$$\ln\frac{1 - DO_0}{1 - DO} = k_L a \cdot t\,, \qquad (3.7)$$

where DO_0 and DO are initial and instantaneous dissolved oxygen percentage, respectively. Defining

$$E = \frac{DO - DO_0}{1 - DO_0}, \qquad (3.8)$$

Eq.3.7 can be written in terms of E as

$$-\ln(1-E) = k_L a \cdot t, \qquad (3.9)$$

when take time lag time t_E into consideration, Eq. 3.9 can be further modified as:

$$-\ln(1-E) = k_L a \cdot t + \ln(1 - t_E k_L a) \qquad (3.10)$$

After data processing and point-linearization, oxygen mass transfer coefficient ($k_L a$) can be read from the slope of the straight line as shown in Fig.3.6. An average value of $k_L a$ within $\pm 10\%$ was obtained with duplicate or triplicate measurements.

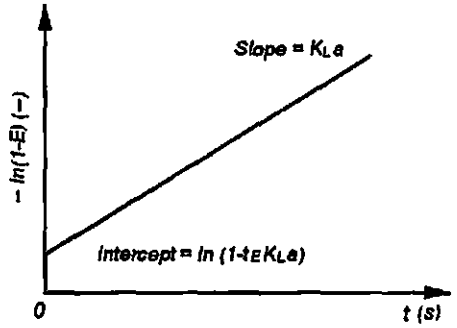

Fig.3.6 Measurement of oxygen mass transfer ($k_L a$)

3.2.5 Molecular diffusion of organic acids through filter walls

The shell-side compartment was filled up with a fermentation solution

containing lactic acid (16.8 *g/L*) and acetic acid (6.3 *g/L*). An external circulation (10*L* acid solution as shown in Fig. 3.1) was provided for good mixing. The tube-side compartment was filled with a mineral solution containing no organic acids. Solution samples were taken at an interval of 1 hour to monitor the change of organic acid concentrations in the two compartments*. The acids were measured with a HPLC equipped with a premier C18 column kept at 60 °C (Shimadzu, Japan). The organic acids were eluted by a water-sulfuric acid solution (pH 2.5) at 0.8 *mL/min*, and detected at UV 210 *nm*. The concentrations were calibrated against standard solutions of pure acids.

Assuming a quasi-steady-state diffusion through the porous walls of membrane tube (Fig. 3.7), Eq. 3.11 gives a mass balance and concentration change with time for lactic acid.

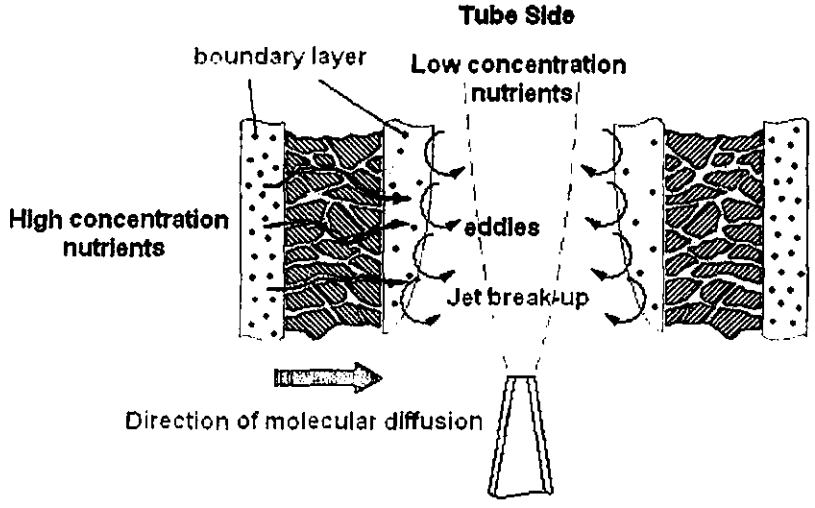

Fig. 3.7 Schematic diagram of molecular diffusion of organic acids through filter walls

* See Appendix C for details

$$N_{LA} = A \cdot D_{LA,e} \frac{(C_{LA,s} - C_{LA,t})}{\delta \cdot V_L} = \frac{dC_{LA,t}}{dt} \qquad (3.11)$$

and $D_{LA,e} = \frac{\xi \cdot D_{LA}}{\tau}$ (3.12),

where N_{LA} is the moles of lactic acid transferred from the shell-side to the tube-side per volume per second, A is the total membrane surface area (0.62 m^2), $D_{LA,e}$ is the effective diffusivity of lactic acid (m^2/s), δ the wall thickness of the filter tubes (m), V_L the liquid volume of tube-side compartment (m^3), $C_{LA,s}$ and $C_{LA,t}$ refer to the lactic acid concentrations in the shell-side and tube-side ($mole/m^3$), respectively. The effective diffusivity of lactic acid depends on the diffusivity in water (D_{LA}, m^2/s), the open area fraction of porous wall (ξ) and a tortuous path that is greater than the thickness of tube wall (δ) by a factor of τ. The value of $D_{LA,e}$ is obtained from the concentration time course with Eq. 3.13 that is derived from Eq. 3.11

$$D_{LA,e} \cdot t = \frac{\delta \cdot V_L}{A\,(V'+1)} \ln\left(\frac{C^0_{LA,s} - C^0_{LA,t}}{V'C^0_{LA,t} + C^0_{LA,s} - V'C_{LA,t} - C_{LA,t}}\right) \qquad (3.13),$$

where V' is the ratio of tube-side volume to shell-side volume. The same method is also used for the effective molecular diffusivity of acetic acid.

Chapter 4. RESULTS AND DISCUSSION

4.1 Gas holdup in riser(s)

The gas holdup in risers is the driving force of liquid circulation in air-lifting reactors. Fig. 4.1a shows a linear increase of gas holdup in individual risers (ε_r) with the riser-based superficial gas-velocity ($U_{G,r}$) under three operation conditions, respectively.

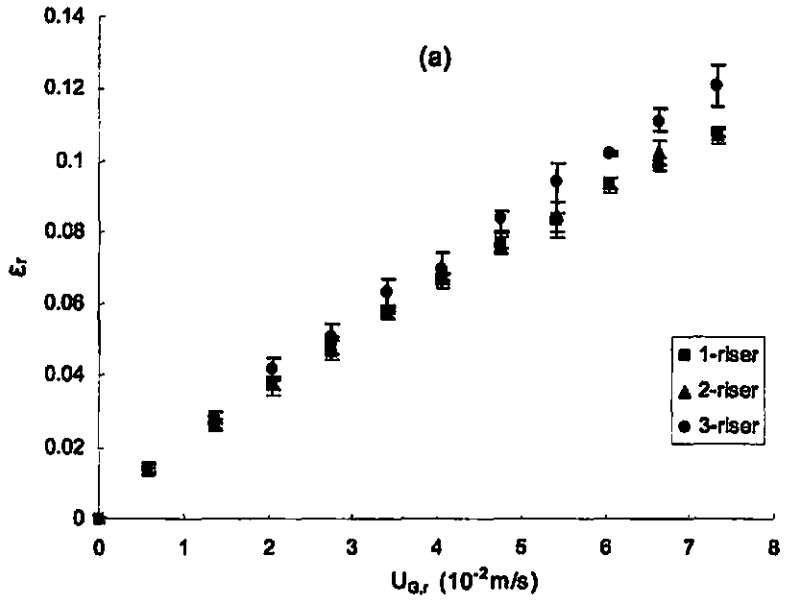

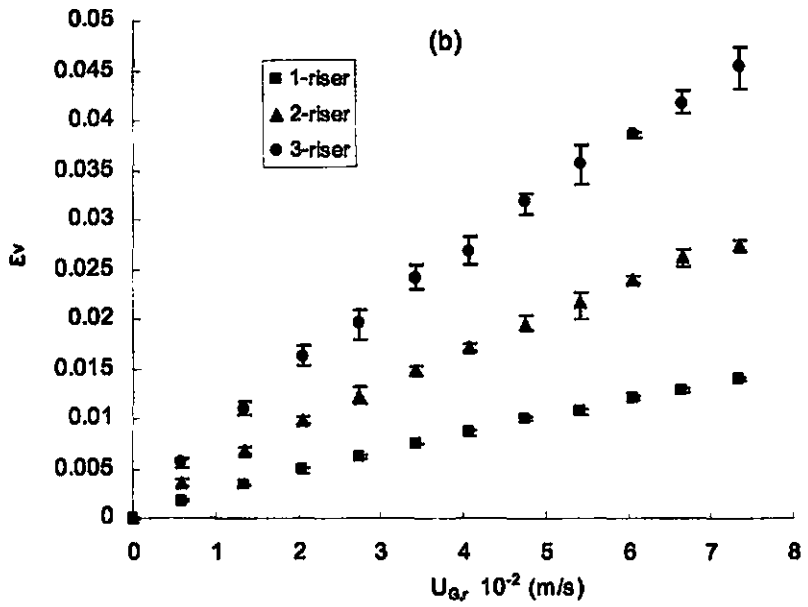

Fig.4.1. Effect of riser-based superficial gas velocity on the gas holdups with one, two and three risers, respectively: (a) gas holdup in individual risers, and (b) the overall gas holdups in the aerobic compartment.

At low gas velocities ($U_{G,r} < 0.04$ *m/s*), the difference of gas holdup under three operation conditions was quite small. It indicates that the individual risers performed independently under multiple air-lifting conditions and the gas holdup in one riser was determined by its aeration rate, not by aeration in other risers. After the superficial gas velocity exceeded 0.06m/s, however, a clear trend of higher gas holdup was observed when three risers were operated, in comparison with one or two risers .This observation indicates that at high aeration rate the gas holdup is to some extent affected by the operation conditions such as the numbers of riser and downcomer. Most likely, when three risers were operated with one downcomer, the ratio of

downcomer-to-riser cross sectional area (A_d/A_r) was the smallest (0.33), and the liquid velocity in the downcomer approached the maximum value at high gas velocities ($U_{G,r}$ = 0.06 *m/s*). It was observed that under this condition, further increase in aeration rate did not increase the liquid flow rate, but generated small air bubbles. The relatively high gas holdup with three risers was, therefore, resulted from the increase in air bubbles and their extended retention time in the risers. The effect of liquid velocity on gas holdup in riser has also been observed by other investigators (Bendjaballah et al. 1999; Choi 2002; Vial et al. 2002).

Gas holdup is also an important parameter for oxygen mass transfer in air-lifting bioreactor. As shown in Fig. 4.1b, the vessel-based gas holdup (ε_v) increases with the aeration rate of individual risers as well as the number of risers. When the operation mode was shifted from one riser to three risers, the measurement error also increased because of the high turbulence and fluctuation of fluid flow. The result shows that the oxygen mass transfer of this multiple air-lifting bioreactor can be easily controlled according to the desired respiration rate of biological systems by adjusting the aeration rate of individual risers, the number of risers, or both. In comparison, a conventional internal or external air-lifting bioreactor with one riser and one downcomer has a fixed A_d/A_r, and air flow rate is the only operational parameter to meet the demands of good mixing, less shear stress and different respiration rates. Many times,

it cannot satisfy all these demands. An unique property of multiple airlifting bioreactor is its operational flexibility by controlling gas velocity, number of risers, or both.

In conventional internal air-lifter, investigators have observed that the overall gas holdup increases and levels off with gas velocity (Chisti 1989; Vial et al. 2002). This phenomenon is attributed to the increased gas holdup in downcomer at high gas flow rate (Chisti 1989; Choi 2002). In contrast, the gas holdup of MAMBR increases almost linearly with superficial gas velocity. This fact suggests an efficient degassing and a low gas holdup in downcomer because of the separated risers and downcomers.

4.2 Gas hold-up in downcomer(s)

Fig. 4.2 gives the gas holdup in downcomer(s) when the reactor is operated with two and three risers, respectively. The gas holdup in downcomer(s) is mainly caused by dissolved air or tiny air bubbles that are brought into the downcomers by liquid circulation before they leave the degassing zone. The tiny bubbles, once they are formed, hardly escape from the downcomers because of the downward liquid flow, particularly when the reactor is operated with three risers and one downcomer at high aeration rates. The gas holdup in downcomer could adversely affect the liquid circulation, mixing, mass transfer of air lifting bioreactors. In the worst conditions,

however, the gas holdup in downcomer(s) is less than 10% of those in the risers by comparing Figs. 4.1a and 4.2.

The liquid degassing in the top degassing zone could be affected by the distance and flow direction between risers and downcomers. For two risers, the downcomers could be arranged in two positions relative to the risers, a parallel position (P1) and a diagonal position (P2) as shown in Fig. 3.1. Fig. 4.2 reveals that the two positions (P1 vs P2) have no statistical difference in downcomer gas holdup. This observation implies a high degassing efficiency of the multiple airlifting risers and downcomers that are separated from each other. In contrast, a conventional internal lifter usually has a high gas holdup in downcomer because of relatively poor degassing efficiency (Chisti 1989)

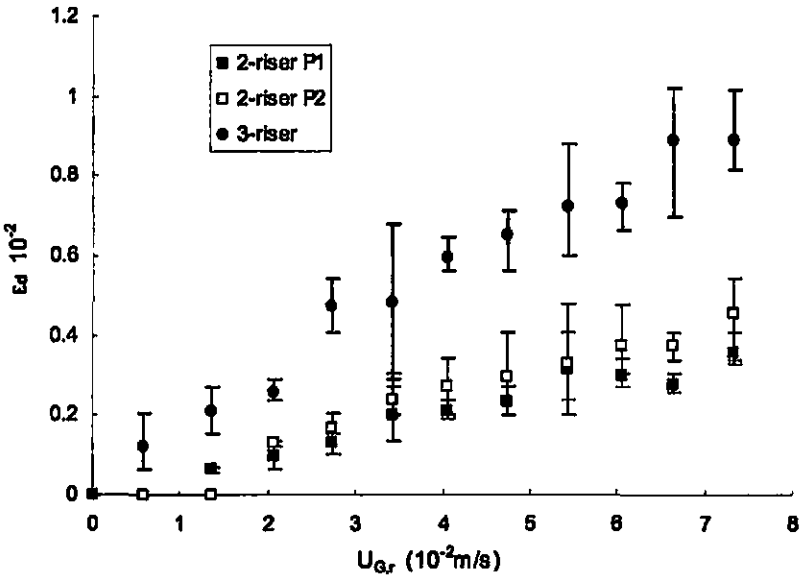

Fig.4.2. The gas holdup (ε_d) in individual downcomer(s) with two and three risers at different riser-based superficial gas velocities ($U_{G,r}$). For two risers, the two downcomers had two positions relative to the risers, parallel position (P1) and diagonal position (P2).

4.3 Superficial liquid velocity in downcomer(s)

Under the driving force of gas holdup difference between the risers and downcomers, the overall liquid circulation in MAMBR could be monitored by measuring the superficial liquid velocity ($U_{L,d}$) in the downcomer(s). Fig. 4.3 gives the measured liquid velocity at different superficial gas velocity ($U_{G,r}$) with one, two and three risers, respectively. It is interesting to note that with one or two risers, the liquid velocity in downcomers increased almost linearly with gas velocity. Under three risers, however, it approached a maximum value around 0.6 *m/s*. In addition, larger increase in liquid velocity was observed when the number of risers was increased from one to two than two to three, even though each riser was operated at the same gas velocity. It should be pointed out that with increasing of riser numbers (m), the number (n) of downcomers was reduced correspondingly ($m + n = 4$). As the ratio of cross section areas of downcomers to risers (A_d/A_r) was linearly reduced from 3 to 1 and further to 0.33, the liquid velocity in downcomers at a given gas velocity would also increase linearly, under an almost constant gas holdup difference between the risers and downcomers (Figs. 4.1a and 4.2). The non-linear increase of liquid velocity with number of risers, therefore, might be attributed

to the increasing energy loss or flow resistance under high turbulence and liquid velocity. It is further found that the liquid velocity in individual risers is substantially lower with three risers than those with one or two risers (data not shown here).

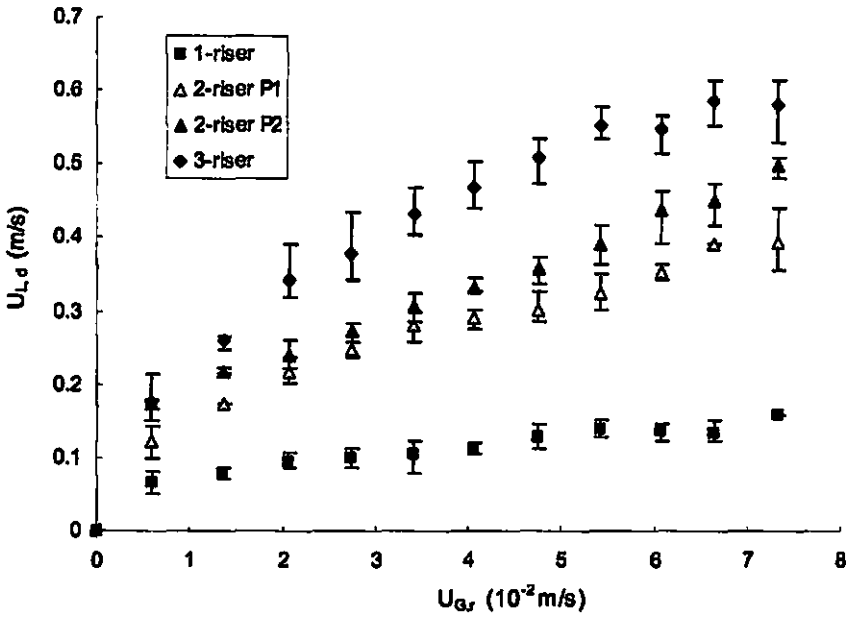

Fig.4.3. The superficial liquid velocities in downcomer(s) ($U_{L,d}$) at riser-based gas velocity ($U_{G,r}$) with one, two and three risers, respectively. For operation of two risers, the liquid velocities were measured in two downcomers that were located at different positions relative to the riser(s), parallel position (P1) and diagonal position (P2).

Fig. 4.3 also shows that with two risers and two downcomers, the parallel arrangement (P1) gave lower liquid velocity than the diagonal arrangement (P2), particularly at high aeration rates. Compared to the diagonal position, the parallel position of risers and downcomers had not only longer flow path but also stronger mixing of fluids in the top and bottom zones, which resulted in a

higher energy loss.

Liquid circulation velocity in air-lifter is a crucial operational parameter that affects the performance of bioreactors, such as mixing time (Merchuk et al. 1996), oxygen mass transfer (Sotiriadis et al. 2005), downcomer gas holdup (Chisti 1989), flow regime transition (Bendjaballah et al. 1999), and adhesive strength of biofilms (Chen et al. 2005). The maximum liquid velocity under three risers, observed at high gas velocities, may be attributed to the energy loss of fluid flow, and/or a constant gas holdup difference between the riser(s) and downcomer(s). The former, as shown by the results above, might be the major factor. Actually, the latter was linearly increased from 0 to 0.1 (compare Figs 4.1a and 4.2). In conventional airlifters, an upper limit of liquid velocity in downcomer is often attributed to a reduced gas holdup difference (Chisti 1989). Our result shows that the liquid velocity can also be limited due to energy loss of liquid circulation.

4.4 Circulation time and mixing time

Liquid mixing in airlifters depends to a great extent on the overall liquid circulation between the risers and downcomers. Fig. 4.4 is the time courses of solution pH after a pulse acid tracer was introduced into the multiple airlifter that was aerated steadily at three rates with one, two and three risers, respectively. As expected, the time required to reach new steady state of

solution pH gets short with increase in gas velocity and risers, because of increase in liquid velocity as discussed above. With one or two risers, the peaks of solution pH could be clearly observed, particularly at low gas velocities, while with three risers the response curves became quite smooth. It demonstrates that this multiple air-lifting bioreactor has a quick and smooth control on solution pH.

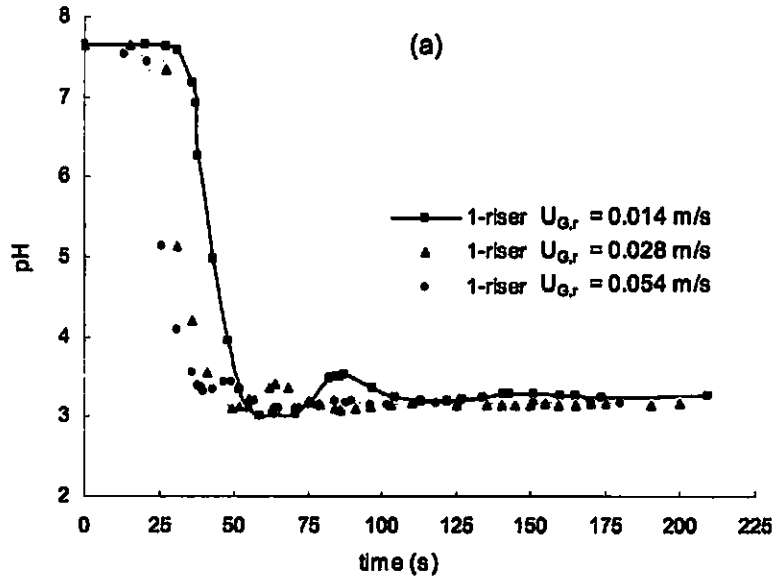

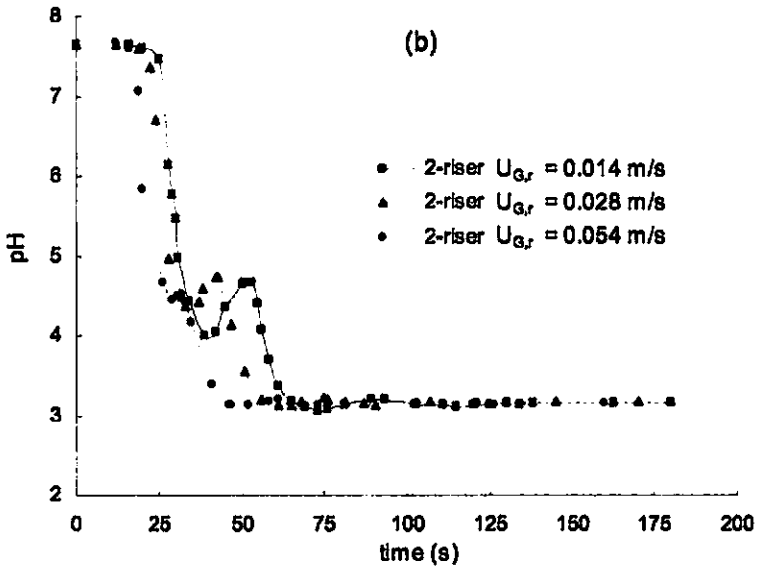

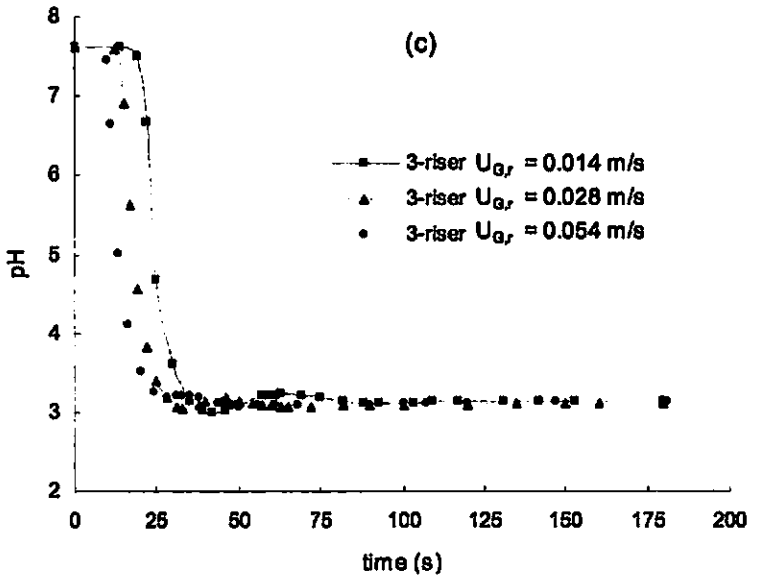

Fig.4.4. The response curves of solution pH to a pulse input of acid tracer at three aeration rates: (a) one riser; (b) two risers; (c) three risers.

From the time gap between the first two peaks of response curves (Fig. 4.4 a & b), the circulation time of overall liquid flow is estimated and given in Table 4.1. The circulation time is reduced from 55 seconds with one riser at a low gas

velocity ($U_{G,r}$=0.014m/s) to 23 seconds with two risers at high gas velocity ($U_{G,r}$=0.054m/s). An ideal circulation time is also calculated by using the liquid velocity in the downcomers ($U_{L,d}$) with the following equation:

$$t_c = \left(2m \cdot V_t + V_{top} + V_{bot}\right) \cdot \frac{1}{U_{L,d} \cdot A_d} \qquad (4.1)$$

where A_d refers to the total cross section area of downcomers, and V_t, V_{top} and V_{bot} to the volumes of downcomers, top degassing zone and bottom distribution zone, respectively. Eq. 4.1 assumes an ideal plug flow of a liquid circulation loop without backmixing, local turbulence, overall dispersion and so on. As shown in Table 4.1, the ideal circulation time has a similar trend with regarding to the effects of number of risers and gas velocity. Generally speaking, the circulation time from tracer response curves is about 2 times longer than the ideal one. In actual liquid circulation, the time is extended because of non-plug flow conditions such as local backmixing, and dead zones near the sudden changes of cross section and flow direction.

Table 4.1. Liquid circulation times estimated from the tracer response curves (Fig.4.4) and with Eq. 4.1.

Number of Riser(s)	Gas velocity [a] $U_{G,r}$ (10^{-2}m/s)	From tracer response Fig. 5 t_c (s)	With Eq. 8 t_c (s)
1	1.35	55	27
1	2.75	42	21
1	5.43	33	18
2	1.35	36	24
2	2.75	30	13
2	5.43	23	10
3	1.35	-[b]	16
3	2.75	-[b]	11

3	5.43	-[b]	8

a. The same superficial gas velocities in individual risers for multiple risers.
b. Not measured.

The mixing performance of an airlifting bioreactor is usually characterized by a mixing time that is defined as the time required to reach a steady state concentration (e.g. 95% homogeneity) after a pulse of tracer is introduced. Verlaan and his coworkers (1989) suggested a correlation between the mixing time (t_m) and liquid circulation time (t_c):

$$\frac{t_m}{t_c} = 0.093Pe = 0.093\frac{U_L L_c}{E_L} \qquad (4.2)$$

where Pe is an overall Peclet number, U_L the mean liquid circulation velocity, L_c the average length of one circulation loop, and E_L the overall axial dispersion coefficient. The overall Peclet number of liquid circulations ranged between 40 and 60 and increased with gas flow rate (Verlaan et al. 1989). For the turbulent liquid and gas flow in this study, Eq. 4.3 is recommended by Joshi et al.(Joshi et al. 1990) to estimate the value of E_L that depends on the diameter (d_t) and liquid velocity ($U_{L,d}$) of downcomers.

$$E_{L,d(r)} = 0.25 \cdot d_t U_{L,d(r)} \qquad (4.3)$$

At superficial gas velocities from 0.014 and 0.054 m/s, the mixing time of this multiple airlifter is reduced from 10.8 to 6.4 min with one riser and from 6.2 to 4.2 min with two risers. These estimated mixing times, however, are much longer than those found with the tracer response curves (Fig.4.4). Actually, it took less than 3 min to reach a new steady pH level after an aliquot of acid

solution was added.

4.5 Oxygen mass transfer (k_La)

The specific volumetric oxygen mass transfer rate (k_La) in MAMBR depends on the number of risers and their aeration rates as shown in Fig.4.5. The oxygen mass transfer from air to water mainly occurs in the risers because of the relatively low gas holdup in downcomers (comparing Figs. 4.1a and 4.2). The mass transfer coefficient of whole airlifter is, therefore, proportional to the number of risers. At a riser-based superficial gas velocity from 0.013 to 0.075m/s, k_La is increased by 3 folds with the increase of risers from 1 to 3. In addition, its increase with superficial gas velocity ($U_{G,r}$) is also in good agreement with the linear increase of gas holdup as shown in Fig. 4.1a.

Usually, liquid circulation velocity is also considered an important factor on the value of k_La. High liquid circulation velocities, for example, may help disperse air bubbles, reduce their coalescence, and improve the interfacial contact between gas and liquid. This positive effect of liquid circulation on oxygen mass transfer, however, is often associated with high gas velocities. For a conventional airlift with a fixed riser/downcomer ratio, it is impossible to identify the individual effects of gas holdup and liquid circulation, because both of them are determined by gas velocity. Our result shows that, the effect of liquid velocity is not significant compared to the number of risers and their gas

holdup. First, the value of k_La is increased in proportional to the number of risers, rather than the non-linear increase of liquid velocity as shown in Fig. 4.3. Second, when the liquid circulation velocity approached a plateau at high gas velocities (Fig.4.3), the value of k_La increased almost linearly with gas velocity (Fig. 4.5), implying a minor influence of liquid velocity on oxygen mass transfer. Actually, a bubble column without a large loop of liquid circulation may provide a higher k_La than an airlift does.

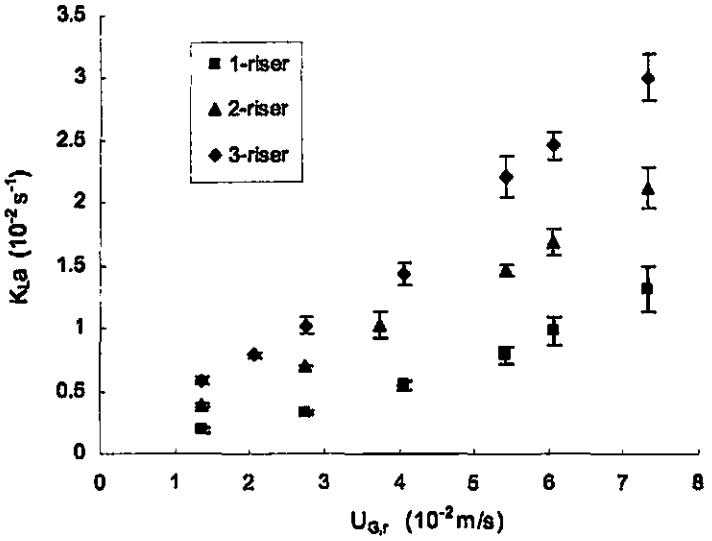

Fig.4.5. Oxygen mass transfer coefficient (k_La) at different riser-based gas velocities ($U_{G,r}$) with one, two and three risers, respectively.

Table 4.2 compares the values of k_La of representative pneumatically agitated bioreactors including a bubble column, an internal airlifter (IL-ALR), two external air-lifters (EL-ALR) and this novel multiple airlifter (MAMBR). The oxygen mass transfer in MAMBR can be controlled in a broad range to meet different respiration rate.

Table 4.2. Comparison of k_La among pneumatically agitated bioreactors in water-air system

Bioreactor	V_L (10^{-2} m^3)	A_r (10^{-2} m^2)	A_d/A_r (−)	Gas sparger	*vvm* (min^{-1})	k_La ($10^{-2}s^{-1}$)	reference
Bubble column	6.96	4.64	—	1*mm*, 106 holes perforated plate	1.0~1.3	2.4~3.0	Chisti (1989)
IL-ALR	1.63	0.54	0.49	Jet-based static mixer	0.5~0.6	1.3~2.1	(Fadavi and Chisti 2005))
EL-ALR (1)	2.60	1.89	0.46	1*mm*, 57 holes	0.4~0.8	0.2~0.5	Kawase (1995)
	2.30		0.20	Perforated plate	0.4~0.8	0.9~1.9	
EL-ALR (2)	1.20	0.62	0.28	1.6mm, 6 holes plate sparger	With packing bed 0.3~0.4	1.7~1.9	Nikakhtari (2005)
					Without packing bed 0.2~0.3	0.4~0.7	
MAMBR	1.63	0.28	3.00	1*mm* Jet	0.4~0.6	0.6~1.0	This work
		0.57	1.00	2 x 1*mm* Jet	1.1~1.3	1.4~1.6	
		0.85	0.33	3 x 1*mm* Jet	1.7~1.9	2.2~2.5	

4.6 Molecular diffusivity of lactic and acetic acids

Four stainless steel filter tubes were used as the multiple riser(s) and downcomer(s) as shown in Fig.3.1. Their porous surface area (0.62 m^2) also let molecules diffuse through the walls under concentration gradients. This multiple-airlifting membrane bioreactor, therefore, can integrate two different biological systems together. For example, simultaneous aerobic and anaerobic fermentations could be performed in the tube-side and shell-side compartments of a single MAMBR, respectively. Fig. 4.6 is the time courses for measurement of diffusivities of two fermentative acids, lactic and acetic

acids, under concentration gradients from the shell-side compartment to the tube-side compartment (see Fig. 3.1 and Fig. 3.7).

The effective diffusivities are obtained from the slopes of linearized curves given by Eq.3.13. For lactic acid, $D_{LA,e}$=6.77x10^{-11} m^2/s (R^2=0.9974) and for acetic acid, $D_{AC,e}$=5.74x10^{-11} m^2/s (R^2=0.97), a semi theoretical equation (Geankoplis 2004) gives the diffusivities of lactic and acetic acids in diluted aqueous solutions of 9.964x10^{-10} and 1.289x10^{-9} m^2/s*, respectively. According to the manufacturer's information, the open area of filter walls (ξ) is about 20% of the overall surface area, and the tortuous factor τ is estimated from the diffusivities of two organic acids. It is found that the molecules of organic acids actually traveled 2.9 to 4.5 times longer path than the wall thickness.

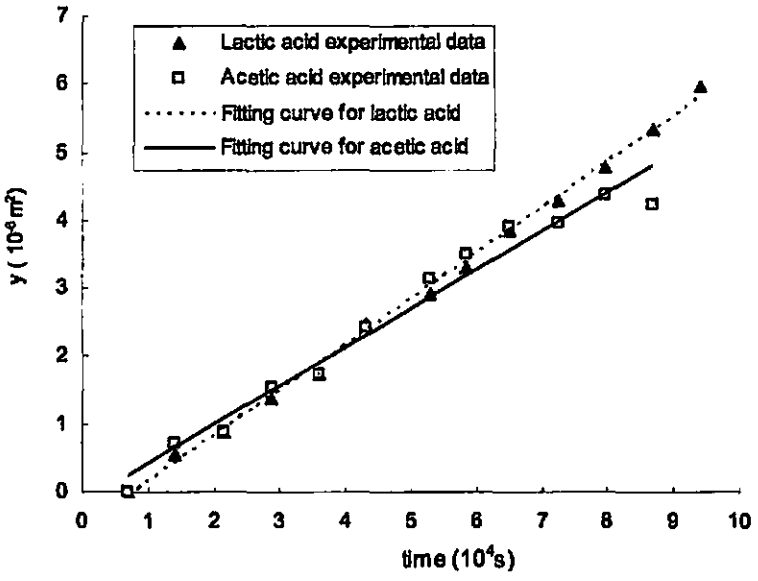

Fig.4.6. Measurement of diffusivity of lactic and acetic acids through the walls of stainless steel filter tubes. The parameter *y* represents the right hand-side of Eq.3.13.

* See Appendix B for details

4.7 oxygen diffusion through membrane tubes

In MAMBR, although aerobic and anaerobic compartment are separated by membrane tubes, it is still possible and worried that dissolved oxygen in aerobic part (tube-side) may diffuse though porous walls of membranes into anaerobic part under concentration gradient and finally negatively affects the performance of anaerobic reactions in the shell-side.

Therefore, experiments were carried out to determine the threshold of the concentration of dissolved oxygen that may result in the diffusion between aerobic and anaerobic compartments.

Initially, dissolved oxygen (DO) in tube-side was first removed by sparging nitrogen gas till the DO concentration near zero. Aeration in shell-side was then begun with different number of risers at different superficial gas velocities and course of tube-side DO change with time was monitored simultaneously.

It is interesting to find that even under the highest aeration rate (~2*vvm*), independent, 3 times repeated experiments of 30-minute consecutively air sparging in shell-side all showed no effects on DO in tube-side. One possible explanation for this phenomenon is that fine bubbles probably blocked the pores of porous walls without being transported through the membrane since no bubbles were observed in the permeate (Vera et al. 2000).

Supported by the observation of biofilms formed on both sides of the porous walls as shown in Fig. 4.7, the hypothesis of oxygen diffusion through

membrane can further be eliminated.

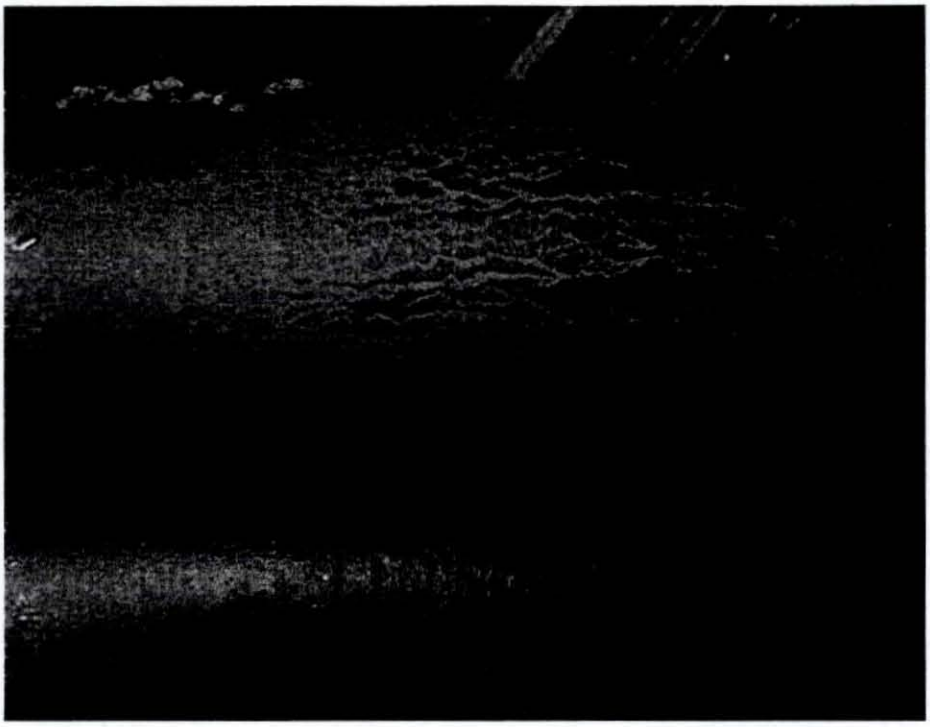

Fig. 4.7 picture of streaked biofilms formed on membrane tubes

Previous researchers have designed a miniature probe that can be mounted into the wall of membrane tubes to test the diffusion of DO through biofilm. Patel and Bott (1991) reported a rapid fall in the amount of oxygen available to the micro-organisms in the layers of biofilm near the interface of testing plate. Besides, they found as the biofilm approached 300μm in thickness, higher liquid velocities across the biofilm had little effect on oxygen availability in the regions near the interface.

Chapter 5. HYDRODYNAMIC MODEL & DIMENSIONAL ANALYSIS

The key factor for successfully scaling up multi-airlifting membrane bioreactor is to reasonably predict the effects of bioreactor geometry, operational conditions and property of fluids on liquid circulation velocity, gas holdup which in turn will to great extent affect mixing time, oxygen mass transfer and molecular diffusion.

In previous studies, the major approach used to predict hydrodynamics of airlift bioreactor was based on empirical correlations due to the complex nature of two-phase flow inside the vessel. As discussed in Chapter 2, those techniques often do not precisely match the case in which we are interested (multiple risers), those correlations are typically valid only for the certain range of conditions used to create the correlation and can only be applied to conventional airlift bioreactor with one pair of riser and downcomer exclusively.

Based on experimental results discussed in Chapter 4, gas holdup in individual risers is found to be independent of liquid circulation and determined by the superficial gas velocity only. Therefore, an empirical equation used to predict gas holdup is correlated with different superficial gas velocities in the first step. Followed by the analysis of pressure balance over a multi-airlifting loop, the predicted value of liquid circulation can be solved through an iterative

process.

In order to achieve the similar performance of biosystems' cultivation and maintain the dynamic similarity after scaling bioreactor from lab- to industry-scale, related nondimensional parameters should not be changed too much during the process of scaling up. Based on Buckingham's Pi theorem, groups of nondimensional parameters are recommended for scaling up MAMBR.

5. 1 Superficial Liquid velocity prediction model

An overall pressure balance is used for the prediction of the riser superficial liquid velocity. The basis of the balance is to equate the pressure differential (ΔP) between the riser(s) and the downcomer(s), which is the driving force that causes liquid circulation to the sum of pressure loss ($\Sigma \Delta P_f$) due to frictions along the flow paths. This approach to solve liquid circulation velocity has been proposed by many previous researchers (Cockx et al. 1997; 2005; Freitas et al. 1999; Heijnen et al. 1997; Hwang and Cheng 1997; Lu et al. 1995).

ΔP is given by

$$\Delta P = \{[\rho_L(1-\varepsilon_d)+\rho_G\varepsilon_d]-[\rho_L(1-\varepsilon_r)+\rho_G\varepsilon_r]\}gh_D \qquad (5.1)$$

where ε_r and ε_d are the gas holdup in riser(s) and in downcomer(s), respectively; h_D is gas-liquid dispersion height.

Since the liquid density (ρ_L) is much larger than gas density (ρ_G), above equation can be further simplified into following form:

$$\Delta P = (\varepsilon_r - \varepsilon_d)\rho_L g h_D \qquad (5.2)$$

The total pressure loss ($\Sigma \Delta P_f$) in the airlift reactor can be further divided into several terms according to different section of MAMBR.

5.1.1 Pressure loss caused by friction

In MAMBR, the riser(s) and downcomer(s) are composed of different combination of several identical porous tubes in which friction loss plays an important role with respect to overall flow. Differing from conventional airlift bioreactors with only one pair of the riser and downcomer, friction loss of tubular flow should not be neglected in MAMBR.

Pressure losses, $\Delta P_{fr(d)}$, originate from the friction between the fluid phase and inner wall of tubes, both in the rise(s) and in the downcomer(s). The fluid phase is a gas-liquid mixture in the riser(s), therefore, effects of two phase flow should be taken into consideration. Given that the gas holdups in the downcomer(s) are rather small compared to that in the riser(s), single-phase equation is used to predict the pressure loss in the downcomer(s).

In the m risers of MAMBR, friction factor f_r, is defined as the drag force per wetted surface unit area (shear stress τ_s at the surface) divided by the product of density times velocity head, $\rho_L v^2/2$. For all the m risers, overall

wetted surface area equals to $m \cdot \pi \cdot d_t \cdot l$, therefore, from friction factor,

$$f_r = \frac{\tau_s}{\rho_L v^2/2} = \frac{\Delta P_{fr} \pi d_t^2}{m \cdot \pi \cdot d_t \cdot l} \Big/ \frac{\rho_L v^2}{2}$$, after rearranging,

For overall pressure loss in *m* riser(s):

$$\Delta P_{fr} = m \cdot 2 f_r \cdot \rho_L \cdot U_{L,r}^2 \frac{l}{d_t} \cdot \phi_L^2 \qquad (5.3)$$

Similarly, for overall pressure loss in *n* downcomer(s):

$$\Delta P_{fd} = n \cdot 2 f_d \cdot \rho_L \cdot U_{L,d}^2 \frac{l}{d_t} \qquad (5.4)$$

where ϕ_L^2, two-phase friction multiplier (Wallis 1969) defined as the ratio of the frictional pressure drop for two-phase flow to that for the single phase liquid flow, is equal to $1/(1-\varepsilon_r)^2$; l, the length of the riser/downcomer; d_t, inside diameter of individual riser/downcomer; $f_{r(d)}$, friction factor, for laminar flow, where Re<2000, $f_{r(d)} = 64/\mathrm{Re}$, in turbulent zone of the Moody diagram, fanning factor is calculated as follows (Swamee and Jain 1976),

$$f_{r(d)} = \frac{0.25}{\left[\log\left(\frac{1}{3.7(d_t/e)} + \frac{5.74}{\mathrm{Re}^{0.9}}\right)\right]^2} \qquad (5.5)$$

and, $\mathrm{Re} = \frac{\rho_L U_{L,r(d)} d_t}{\mu_L}$, ranging from 5×10^3~1×10^8 (5.6)

where d_t/e, is the relative roughness of inside wall of the riser/downcomer, ranging from 100 to 1×10^6. From Binder (1973), *e* is the average size of the bumps on the wall of porous tube, and cast iron (e=0.26*mm*) was chosen for prediction.

$U_{L,r}$ and $U_{L,d}$ in Eq 5.3 and 5.4 are the superficial liquid velocities in the riser(s) and the downcomer(s), respectively.

5.1.2 Pressure loss caused by change in cross-section area

There are two types of diameter changes in this MAMBR, one is "sudden contraction" and the other is "sudden expansion", both of which occurred at either the top or the end of riser(s) and downcomer(s), depending on the direction of liquid flow. Geankoplis (2004) proposed that, the friction coefficient can be calculation as follows:

$$\textit{For sudden expansion: } K_{S,E} = \left(1-\frac{d_t^{\,2}}{D_{app}^{\,2}}\right)^2 = \left(1-\frac{0.06^2}{0.1136^2}\right)^2 = 0.520 \qquad (5.7)$$

$$\textit{For sudden contraction: } K_{S,C} = 0.55\left(1-\frac{d_t^{\,2}}{D_{app}^{\,2}}\right) = 0.397 \qquad (5.8)$$

where D_{app} is the apparent diameter of sudden expansion/contraction section as defined in Fig. 5.1.

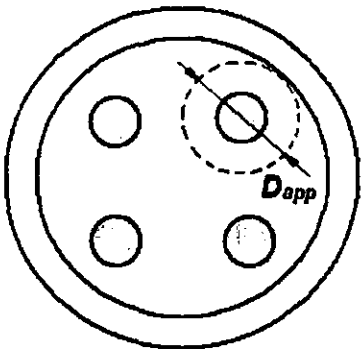

Fig. 5.1 Schematic diagram of the definition of apparent diameter (D_{app})

Those two parts of the pressure losses are called "minor loss" compared

with friction loss in applied fluid mechanics. Therefore, from engineering point of view, it would be good enough to predict the pressure drop caused by sudden expansion and contraction based on single phase, liquid flow.

Due to the fact that pressure loss caused by diameter change is proportional to the number of sections where diameter change happens, therefore in MAMBR with *m* riser(s) and *n* downcomer(s), overall pressure loss caused by diameter change can be written as:

$$\Delta P_{S,E} + \Delta P_{S,C} = \frac{1}{2}\rho_L \left[V_{L,r}{}^2 \left(K_{S,E} + K_{S,C} \right) \cdot m + V_{L,d}{}^2 \left(K_{S,E} + K_{S,C} \right) \cdot n \right] \qquad (5.9)$$

where $V_{L,r}$ and $V_{L,d}$ are the true linear liquid velocities or the interstitial velocities in the riser(s) and the downcomer(s), respectively, and are related to the corresponding superficial velocities in the following equation:

$$V_{L,r(d)} = \frac{U_{L,r(d)}}{1 - \varepsilon_{r(d)}} \qquad (5.10)$$

for $\varepsilon_d = 0$, $V_{L,d} = U_{L,d}$.

5.1.3 Pressure loss caused by change in flow direction

In MAMBR, all the exits/entrances of riser(s) and entrances/exits of downcomer(s) are connected in one common top/bottom section, where overall direction of liquid circulation changes. As shown in Fig.3.1, geometric configurations of the top/bottom of MAMBR is similar to that of internal-loop airlift reactors investigated in Chisti's work(1989). Therefore, following equation is used to calculate the friction factors in the top and the bottom of

MAMBR:

$$K_{T(B)} = 11.40\left(\frac{A_t}{A_{top(bot)}}\right)^{0.79} \qquad (5.11)$$

valid for an A_t/A_b range of 0.2~1.8. Where A_t is cross-sectional area of single membrane tube based on the inside diameter; $A_{top(bot)}$ is the free area above/below the separation plate of the top/bottom as shown in Fig. 3.1

For overall pressure loss caused by flow direction change,

$$P_T + \Delta P_B = \frac{1}{2}\rho_L\left[V_{L,r}{}^2 \cdot K_T \cdot m + V_{L,d}{}^2 \cdot K_B \cdot n\right] \qquad (5.12)$$

At steady state:

$$\begin{aligned}\Delta P &= \sum \Delta P_f \\ &= \Delta P_{fr} + \Delta P_{fd} + \Delta P_{S,E} + \Delta P_{S,C} + P_T + \Delta P_B\end{aligned} \qquad (5.13)$$

Furthermore, the continuity equation for the liquid flow between the riser and downcomer can be written as:

$$A_r \cdot U_{L,r} = A_d \cdot U_{L,d} \qquad (5.14)$$

where $A_{r(d)}$ is the total cross sectional area of risers/downcomer(s).

Finally, the substitution of Eq.5.2~5.12 and Eq.5.14 into Eq.5.13 yields the following expression for the riser superficial liquid velocity:

$$\begin{aligned}&(\varepsilon_r - \varepsilon_d)\rho_L g h_D \\ &= m \cdot 2f_r \cdot \rho_L \cdot (U_{L,r})^2 \frac{l}{d_t} \cdot \phi_L^2 + n \cdot 2f_d \cdot \rho_L \cdot \left(\frac{A_r}{A_d}\right)^2 (U_{L,r})^2 \frac{l}{d_t} \\ &+ \frac{1}{2}\rho_L\left[\left(\frac{U_{L,r}}{1-\varepsilon_r}\right)^2 (K_{S,E} + K_{S,C}) \cdot m + \left(\frac{A_r}{A_d}\right)^2 \left(\frac{U_{L,r}}{1-\varepsilon_d}\right)^2 (K_{S,E} + K_{S,C}) \cdot n\right] \\ &+ \frac{1}{2}\rho_L\left[\left(\frac{U_{L,r}}{1-\varepsilon_r}\right)^2 \cdot K_T \cdot m + \left(\frac{A_r}{A_d}\right)^2 \left(\frac{U_{L,r}}{1-\varepsilon_d}\right)^2 \cdot K_B \cdot n\right]\end{aligned} \qquad (5.15)$$

After rearranging, it gives,

$$U_{L,r} = \left(\frac{2(\varepsilon_r - \varepsilon_d) g h_D}{\left[m \cdot \left(4 f_r \cdot \frac{l}{d_t} \cdot \phi_L^2 + \frac{K_{S,E} + K_{S,C} + K_T}{(1-\varepsilon_r)^2} \right) + n \cdot \left(\frac{A_r}{A_d} \right)^2 \left(4 f_d \frac{l}{d_t} + \frac{K_{S,E} + K_{S,C} + K_B}{(1-\varepsilon_d)^2} \right) \right]} \right)^{0.5}$$

(5.16)

where h_D is gas-liquid dispersion height, it can be estimated by using following equations:

$$h_D = \frac{h_L}{1-\varepsilon_D} \qquad (5.17)$$

and $$\varepsilon_D = \frac{A_r \varepsilon_r + A_d \varepsilon_d}{A_r + A_d} \qquad (5.18)$$

5. 2 Flow regime prediction in the riser of reactor

In Eq.5.16, once the form of prediction equation of gas holdup in the riser(s)/downcomer(s) can be determined, all the items and factors can be solved either by the geometric configurations of the bioreactor or through a regression process beginning with an assumption of liquid velocity.

Flow regime identification is a crucial process before the prediction of gas holdups, because gas holdups will be very different from each others when flow regime changes. Therefore it is necessary to understand flow regime first.

5.2.1 Flow regime classification

When designing devices in which a two-phase flow occurs, the determination of a flow regime is one of the most essential problems. The flow pattern maps (Fig. 5.2) available in literature were first developed for the petrochemical industry (Baker 1954) for flow of oil and gas in large diameter pipes. Different flow regimes may arise, which are depending on the flux of both phases, properties of various factors as well as dimensions and location of a channel (Samaras and Margaris 2005).

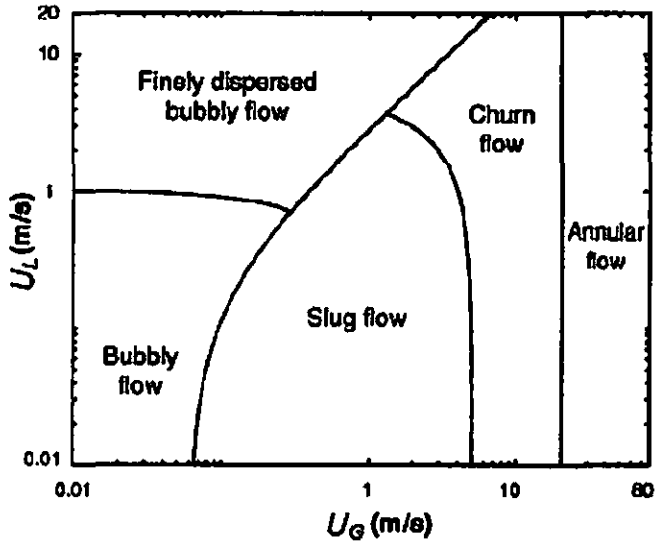

Fig. 5.2 Flow regime map for a 72-mm inner diameter vertical pipe flow of air and water according to the model of Taitel (1980)

A very wide variety of flow regimes have been defined in the literature, this results partly from the subjective nature of flow-regime definitions and partly from a variety of names being given to essentially the same regime. Hewitt and Roberts (1969) designated five basic patterns for upflow namely, bubble flow,

slug or plug flow, churn flow, annular flow and wispy-annular flow, defined as follows (Fig. 5.3):

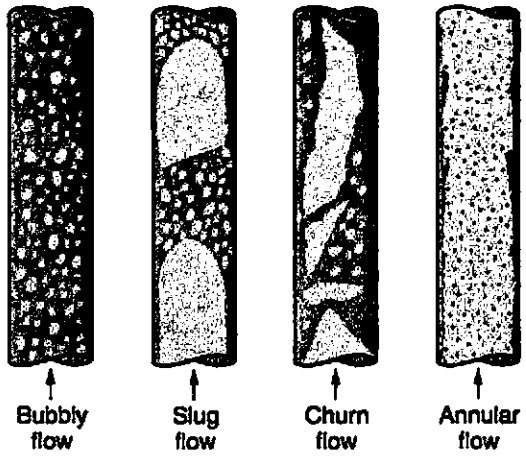

Fig. 5.3 Flow patterns observed in vertical upward bubbly pipe flow (Taitel et al. 1980)

Bubble flow. The liquid is continuous, and a dispersion of bubbles flows within the liquid continuum.

Slug or plug flow. At higher gas flows, bubble coalescence occurs, and eventually the bubble diameter approaches that of the tube. When this occurs, large characteristically bullet shaped bubbles are formed.

Churn flow. With increasing flow velocity, a breakdown of the slug flow bubbles leads to an unstable flow regime in which there is an oscillatory motion of the liquid upward and downward in the tube.

Annular flow. The liquid flows on the wall of the tubes as a film, and the gas phase flows in the centre. Usually, some of the liquid phase is entrained as small droplets in the gas core.

Wispy annular flow. As the liquid flow rate is increased, the concentration of

drops in the gas core increases; ultimately, droplet coalescence in the core leads to large lumps or streaks (wisps) of liquid in the gas core. This regime is characteristic of flows with high flux.

5.2.2. Effect of bubble size on flow regime transition

The selection of the appropriate flow pattern is the key to successful gas holdup predictions because the appropriate modeling approaches are different from one flow pattern to the other(Guet and Ooms 2006). In particular, the bubbly-flow to slug-flow transition is an important issue for air-lift predictions. It was recently reported that the bubble size has strong impact on the bubbly-flow to slug-flow transition in air-water systems. For air-water systems with relatively large bubbles ($0.05 < D_b / D_p < 0.2$) the critical gas holdups associated with flow pattern transition is linearly related to the bubble size (Cheng et al. 2002; Guet et al. 2003; Song et al. 1995). A unique relation is valid for a large range of pipe diameters ($25mm < D_p < 72mm$):

$$\varepsilon_{critical} = 0.55 - 2.37\frac{D_b}{D_p} \qquad (5.19)$$

where D_b is the mean Sauter diameter; D_p is the diameter of testing pipe.

This result suggests that a constant critical gas holdups model, such as $\varepsilon_{critical} = 0.25$ (Taitel et al. 1980) or $\varepsilon_{critical} = 0.3$ (Mishima and Ishii 1984), cannot be generally valid. However, they do can provide a roughly good prediction to at least alleviate the effect of unwanted slug-flow.

In Couvert et al.(1999)'s work, a video camera was used to measure the bubble size. The dimensions of bubbles, generally ellipsoidal, generated by the sparger were measured for four positions in the reactor, and six gas flow rates. The diameter of a bubble (d_{Bl}) was calculated with Eq.5.20; then, the mean Sauter diameter D_b for about 180 bubbles was deduced with Eq.5.21.

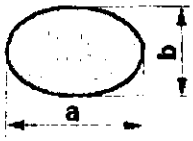

Fig. 5.4 geometric size for calculating mean Sauter bubble diameter

$$d_{Bl} = \left(a^2 b\right)^{1/3} \tag{5.20}$$

$$D_b = \frac{\sum_1^{N_a} d_{Bl}^{\ 3}}{\sum_1^{N_a} d_{Bl}^{\ 2}} \tag{5.21}$$

where *a* and *b* are geometrically defined as shown in Fig.5.3;

5. 3 Empirical equations for gas holdup in riser(s)

The drift-flux model proposed by Zuber and Findlay (1965) has been widely used in the two phase flow literature and accounts for an effective slip between the phases which occurs due to the non-uniform profiles.

Based on the model proposed by Zuber and Findlay (1965), gas hold can be correlated with superficial gas and liquid velocity in the following form.

$$\frac{U_G}{\varepsilon_G} = C_0(U_G + U_L) + C_1 \tag{5.22}$$

where C_0 Indicates the extent of radial non-uniformity in the gas holdup. In the

homogeneous regime, with uniform radial holdup, the value of C_0 is unity and its value increase with an increase in the non-uniformity. C_1 is terminal bubble rise velocity. An expected range for bubble rise velocity in air-water is 0.2~0.3m/s(Chisti 1998).

Although the Eq.5.22 has been widely used to predict the gas holdups in the riser of conventional airlift bioreactors, it can not be applied to MAMBR due to the observation and experimental results that the gas holdups in riser(s) of MAMBR are independent of liquid velocities. Therefore it becomes necessary to correlate the experimental data of gas holdups with gas superficial velocity. This process of empirical correlation is also widely applied for conventional airlift bioreactors(Bello et al. 1984; Choi and Lee 1993; Couvert et al. 1999).

The gas holdup can be correlated as $\varepsilon_r = aU_{G,r}^b$ by

$$\varepsilon_r = 1.61U_{G,r}, \qquad R^2=0.9881 \qquad (5.23)$$

Fig 5.5 compares the experimental data of riser(s) gas holdups with prediction curve based on Eq. 5.23.

The prediction curve well estimates the linear increase of gas holdup in individual risers (ε_r) with the riser-based superficial gas-velocity ($U_{G,r}$) under three operation conditions, respectively. This indicates that the individual risers performed independently under multiple air-lifting conditions and the gas holdup in one riser was determined by its aeration rate, not by aeration in other risers.

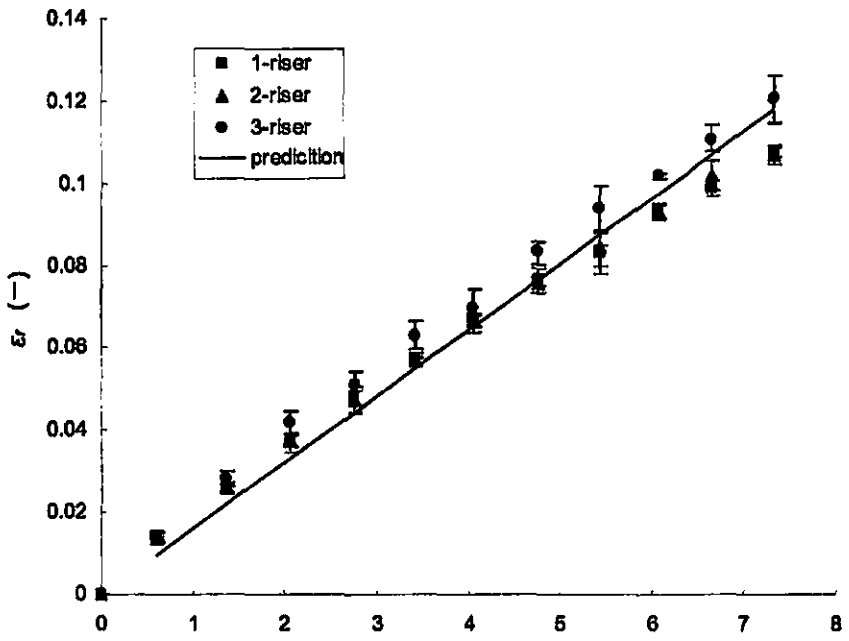

Fig.5.5. Gas holdups in individual risers. Comparison between experimental date and prediction curve based on Eq.5.23.

Based on Eq. 5.14, 5.16 and 5.23, superficial liquid velocities in the downcomer(s) were predicted and compared with experimental data in 3 operation conditions with 1-riser, 2-riser and 3-riser, respectively, as shown in Fig.5.6.

The prediction curves reasonably agree with the trend of liquid velocities increasing with gas flow rate when the number of risers was increased from one to three. However, under three risers, the maximum liquid velocity observed in experiments around $U_{G,r}$=0.65 *m/s* is not estimated obviously.

It is interesting to note that at the same superficial gas velocity ($U_{G,r}$), values of liquid velocities are generally higher on the prediction curves than

those measured in experiments, with 1-and 3-riser. This disagreement is mostly likely induced by ignoring downcomer gas holdups in the process of prediction of liquid velocities. This is supported by the observation discussed in previous chapter, a high degassing efficiency of MAMBR can be achieved in which the multiple airlifting risers and downcomers are separated from each other. In contrast, a conventional internal lifter usually has a high gas holdup in downcomer because of relatively poor degassing efficiency and an reduced liquid velocity in downcomer is often attributed to an increase of downcomer gas holdup (Chisti 1989).

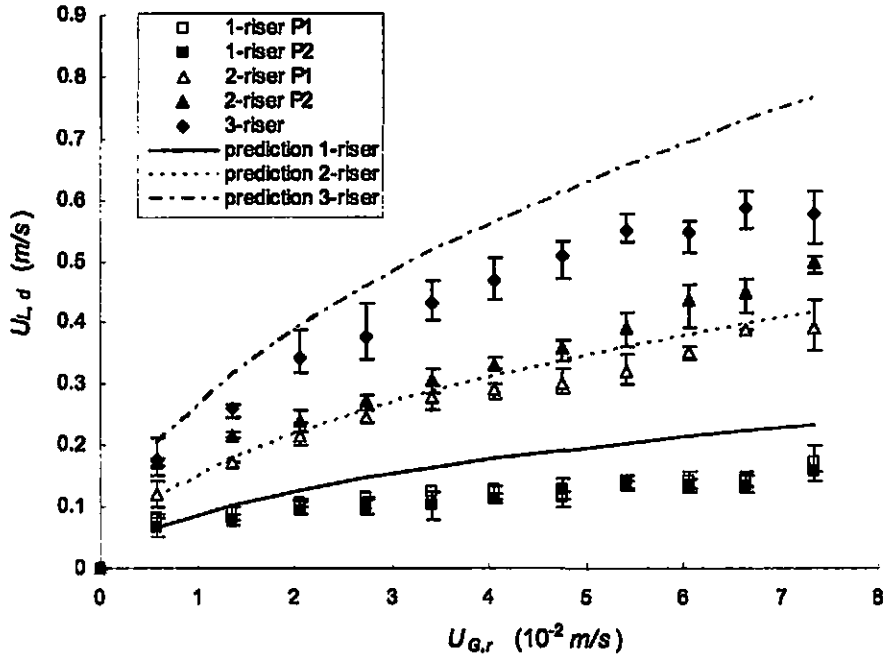

Fig.5.6. The superficial liquid velocities in downcomer(s) ($U_{L,d}$) at riser-based gas velocity ($U_{G,r}$) with one, two and three risers, respectively. For operation of two risers, the liquid velocities were measured in two downcomers that were located at different positions relative to the

riser(s), parallel position (P1) and diagonal position (P2).Comparison between experimental date and prediction curve based on Eq. 5.14, 5.16 and 5.23.

5. 4 Dimensional analysis using the Buckingham method

Important dimensionless numbers can be generally obtained from the basic differential equations of the system. In many cases, it is difficult to formulate a differential equation which clearly applies. Then a more general procedure—Buckingham method is required, as in our investigation on MAMBR. In the first step of this method, all the important variables should be listed. In the next step, by applying the Buckingham pi theorem, we can then determine the number of dimensionless parameters into which the variables may be combined.

5.4.1 Process of deriving dimensionless number:

Three categories of important variables are considered in this study:

Configuration parameters of MAMBR

$A_{r(d)}$, $A_{top(bot)}$, A_m, d_t, D, D/e, $f_{r(d)}$, h_D, h_L, m, n, V_L, V_t, V_{top}, V', δ, τ

Property parameters and constants of MAMBR

ρ_L, μ_L, σ, g, C_L, $C_{LA,t(s)}$

Operation parameters of MAMBR

$U_{G,r}$, $U_{L,d}$, ε_r, ε_d, ΔP, k_La, $D_{LA,e}$

Here we will use the derivation of downcomer Reynolds number as an

example. Consider the pressure drop ΔP in individual downcomer, which is expected to depend on the inside diameter D of the tube, its length l, the average size e of the wall roughness elements, the average flow velocity in the downcomer(s)$U_{L,d}$, the fluid density ρ_L and the fluid viscosity μ_L.

The dimensions of the variables can be arranged in the form of following matrix,

	ΔP	D	l	e	$U_{L,d}$	ρ_L	μ_L
M	1	0	0	0	0	1	1
L	-1	1	1	1	1	-3	-1
T	-2	0	0	0	-1	0	-1

(5.24)

Eq. 5.24 is called a dimensional matrix. The rank r of any matrix is defined to be the size of the largest square submatrix that has a nonzero determinant. In most problems in fluid mechanics without thermal effects, r=3. According to Buckingham's pi theorem, since there are totally 7 variables related to the liquid flow inside MAMBR's downcomer(s), the number of nondimensional parameters must be $n - r = 4$.

For pipe flow problem, 3 repeating variables $U_{L,d}$, D and ρ_L are chosen to build up 4 nondimensional products. The first dimensional product can be taken as:

$$\Pi_1 = U_{L,d}{}^a D^b \rho_L{}^c \Delta P$$

The exponents a, b, and c are obtained from the requirement that Π_1 is dimensionless. This requires,

$M^0L^0T^0 = (LT^{-1})^a(L)^b(ML^{-3})^c(ML^{-1}T^{-2}) = M^{c+1}L^{a+b-3c-1}T^{-a-2}$,

Equating indices, it gives a=-2, b=0, c=-1, so that

$$\Pi_1 = U_{L,d}{}^{-2} D^0 \rho_L{}^{-1} \Delta P = \frac{\Delta P}{\rho_L U_{L,d}{}^2}$$

Through similar procedures, we obtain

$$\Pi_2 = U_{L,d}{}^a D^b \rho_L{}^c l = \frac{l}{D},$$

$$\Pi_3 = U_{L,d}{}^a D^b \rho_L{}^c e = \frac{e}{D}$$

$$\Pi_4 = U_{L,d}{}^a D^b \rho_L{}^c \mu_L = \frac{\mu_L}{\rho_L U_{L,d} D}$$

It is obvious to find that Π_4 is equal to 1/Re. It is suggested that with some experience, all the nondimensional variables can be found by inspection alone, thus no formal analysis is needed.

5.4.2 Dimensionless number of mass transfer

In MAMBR, mass transport by diffusion and forced convection are influence by the following variables: the mass transfer coefficient k, the molecular diffusivity of the transferring component D, the fluid density ρ, and viscosity μ, a characteristic length d, and the velocity of low U. Mass transfer by natural convection is influence also by the gravitational acceleration g and the density difference $\Delta\rho$ between phases. These variables can be grouped into the following principal dimensionless numbers (Chisti 2005):

$$\text{Re (Reynolds number)} = \frac{\text{inertial force}}{\text{viscous force}} = \frac{\rho_L U_L d}{\mu_L}$$

$$\text{Sh (Sherwood number)} = \frac{\text{total mass transfer}}{\text{diffusive mass transfer}} = \frac{k_L d}{D_L}$$

$$\text{Sc (Schmidt number)} = \frac{\text{momentum diffusivity}}{\text{mass diffusivity}} = \frac{\mu_L}{\rho_L D_L}$$

$$\text{Gr (Grashof number)} = \frac{\text{(inertial force)(bouyancy force)}}{(\text{viscous force})^2} = \frac{d^3 \rho_L \Delta\rho g}{\mu_L^2}$$

$$\text{Fr (Froude number)} = \frac{\text{inertial force}}{\text{gravitation force}} = \frac{U_L^2}{gd}$$

where the subscript *L* denotes the liquid phase. Reynolds number, Sherwood number, and Schmidt number can be written for gas and liquid phases, respectively. The above noted dimensionless numbers represent ratios of various factors that may play a role in a given situation. Grashof number is important in situations where density difference driven natural convection affects mass transfer. Reynolds number is employed in situations where forced convection is the predominant influence on transport processes. Froude number is useful in describing gravity-influenced flows. Schmidt number, ratio of momentum diffusivity to mass diffusivity, is a measure of relative effectiveness of mass and momentum transfer. Some of those dimensionless numbers may be expressed in other forms depending on the situation. Some of other dimensionless numbers relevant to mass transfer and related fluid mechanics are listed below (Chisti 2005):

$$\text{Bo (Bond number)} = \frac{\text{gravity force}}{\text{surface tension force}} = \frac{g d_P^2 \Delta\rho}{\sigma_L}$$

$$\text{Pe (Peclet number)} = \frac{\text{bulk mass transport}}{\text{diffusional mass transport}} = \frac{U_L L}{D_L} \text{ or } \frac{U_G L}{D_G}$$

$$\text{Ps (Poiseuille number)} = \frac{\text{viscous force}}{\text{gravity force}} = \frac{\mu_L U_P}{\rho_L g d_P^{\,2} \Delta\rho} \text{ or } \frac{\mu_G U_P}{\rho_G g d_P^{\,2} \Delta\rho}$$

$$\text{We (Weber number)} = \frac{\text{inertial force}}{\text{surface tension force}} = \left(\frac{U_P^{\,2} \rho_L d_P}{\sigma_L} \right)^{1/2}$$

where the subscript *P* denotes the solid phase (particles).

Chapter 6. CONLUSIONS AND RECOMMENDATIONS

6.1 Conclusions

1. Gas holdup in individual risers (ε_r) increases linearly with the superficial gas-velocity (U_G), and performs independently under multiple air-lifting conditions.

2. The vessel-based gas holdup (ε_V) and liquid velocity in downcomer(s) increase with aeration rate of individual risers as well as the number of risers (n).

3. The liquid velocity in downcomers reaches an upper limit (about 0.6 *m/s*), because of flow resistance, or energy loss of liquid circulation.

4. The oxygen mass transfer coefficient (k_La) is mainly affected by gas holdup and the number of risers, and to some extent by liquid velocity.

5. The novel configuration results in good mixing in the bioreactor that quickly reaches new steady state in response to a sudden pH change from acid addition.

6. It was experimentally proved that dissolved oxygen in aerobic compartment would not obviously diffuse through the walls of membrane tubes into anaerobic compartment.

7. A hydrodynamic multi-airlifting model has been developed for the prediction of the liquid circulation velocity and gas holdup in the riser(s). Comparison between model and experimental data is quite acceptable.

8. Dimensional analysis has been conducted based and several dimensionless numbers are recommended for scaling-up design.

6.2 Recommendations

1. In present study, experiments of effects of air sparging on hydrodynamics in MAMBR were carried out on the basis of identical gas flow rates in all the risers. It is recommended to use different gas flow rates in individual multi-risers to further study the influence of the number of risers and gas flow rates on liquid circulation velocity, mass transfer, mixing time and molecular diffusion.

2. Comparison between model and experimental data of pilot-scale MAMBR is suggested before further attempt to apply the hydrodynamic model on guiding industrial design.

3. Under the driving force of concentration gradient, molecular diffusion of organic acids through membrane tubes has already been tested in present study. More experiments are recommended to further investigate the effects of the thickness of biofilms, liquid circulation velocities and gas sparing on molecular diffusion through membrane tubes.

4. Before final industrialization, in order to reduce the cost of experimental validation of hydrodynamic model in larger scale MAMBR, computer simulation is recommended for visualizing the possible change of flow pattern that may

occur when necessary modification is made.

Notation

A_d	The total cross sectional area of downcomers	(m^2)
A_r	The total cross sectional area of risers	(m^2)
A_t	The cross-sectional area of single membrane tube	(m^2)
A_{top}	Free area above the separation plate of the top section	(m^2)
A_{bot}	Free area below the separation plate of the bottom section	(m^2)
A_m	Overall surface area of four membrane tubes	(m^2)
Bo	Bond number	(—)
C_L	Instantaneous concentration of dissolved oxygen in water	(kgm^{-3})
C_{L0}	Initial concentration of dissolved oxygen in water	(kgm^{-3})
C^*	Saturated concentration of dissolved oxygen in water	(kgm^{-3})
$C^0_{LA,s}$	Initial concentration of shell-side lactic acid	(kgm^{-3})
$C^0_{LA,t}$	Initial concentration of tube-side lactic acid	(kgm^{-3})
$C_{LA,s}$	Instantaneous concentration of shell-side lactic acid	(kgm^{-3})
$C_{LA,t}$	Instantaneous concentration of tube-side lactic acid	(kgm^{-3})
C_P	Dimensionless coefficient of Pitot tube calibration	(—)
d_t	Inside diameter of porous tubes	(m)
D_{app}	Apparent diameter of sudden expansion/contraction	(m)
D_b	The mean Sauter diameter	(m)
D_p	The diameter of testing pipe	(m)

DO	Dissolved oxygen in percentage of saturation	(—)
$D_{LA,e}$	Effective diffusivity of lactic acid in the porous wall of stainless steel filter tubes	(m^2/s)
e	Average size of the bumps on the wall of porous tube	(m)
E	Intermediate parameter equals to $(DO - DO_0)/(1 - DO_0)$	(—)
E_i	Energy input due to isothermal gas expansion	(W)
Er	Energy dissipation due to bubble wakes in the riser(s)	(W)
E_d	Energy loss due to stagnant gas in the downcomer(s)	(W)
E_b	Energy loss (bottom connection)	(W)
E_t	Energy loss (top connection)	(W)
E_{fr}	Frictional energy loss in downcomer	(W)
E_{fd}	Frictional energy loss in riser	(W)
E_L	Overall axial dispersion coefficient	(—)
$E_{L,d}$	Axial dispersion coefficient in individual downcomers	(—)
$E_{L,r}$	Axial dispersion coefficient in individual risers	(—)
f	Fanning factor	(—)
f_r	Fanning factor in the riser(s)	(—)
f_d	Fanning factor in the downcomer(s)	(—)
Fr	Froude number	(—)
g	Gravitational acceleration	(ms^{-2})
Gr	Grashof number	(—)
h_D	Gas-liquid dispersion height	(m)

h_L	Unaerated liquid height	(m)
Δh	Reading difference between two incline manometers	(m)
ΔH	Distance between two Pitot tube ports	(m)
k_La	Volumetric mass transfer coefficient of oxygen in water	(s^{-1})
l	Length of membrane tube	(m)
L_c	Average length of one circulation loop	(m)
m	The number of riser(s)	(−)
n	The number of downcomer(s)	(−)
N_{LA}	Molar flux of lactic acid from shell-side to tube side	($mol/m^3 \cdot s$)
P_h	Bioreactor head-space pressure	(Pa)
Pe	Peclet number	(−)
Ps	Poiseuille number	(−)
ΔP	Pressure drop	(Pa)
ΔP_{fr}	Pressure loss caused by friction in the riser(s)	(Pa)
ΔP_{fd}	Pressure loss caused by friction in the downcomer(s)	(Pa)
$\Delta P_{S,E}$	Pressure loss caused by diameter sudden expansion	(Pa)
$\Delta P_{S,C}$	Pressure loss caused by diameter sudden expansion	(Pa)
ΔP_T	Pressure loss caused by flow direction change on the top section	(Pa)
ΔP_B	Pressure loss caused by flow direction change in the bottom section	(Pa)
Re	Renolds number	(−)
Q	Volumetric flow rate	(m^3s^{-1})

Sh	Sherwood number	(−)
Sc	Schmidt number	(−)
t	Time	(s)
t_E	Tag time	(s)
t_m	Mixing time in the tube-side compartment	(s)
t_c	Circulation time in the tube-side compartment	(s)
$U_{G,r}$	Superficial gas velocity based on the cross sectional area of individual risers	(m/s)
U_L	Mean liquid circulation velocity	(m/s)
$U_{L,av}$	Average liquid circulation velocity based on Eq. 5.24	(m/s)
$U_{L,d}$	Superficial liquid velocity in downcomer(s)	(m/s)
$U_{L,r}$	Superficial liquid velocity in riser(s)	(m/s)
$U_{L,t}$	Superficial liquid velocity in calibration device	(m/s)
$V_{L,r}$	True linear liquid velocity in the riser	(m/s)
$V_{L,d}$	True linear liquid velocity in the downcomer	(m/s)
V_L	The liquid volume of tube-side compartment	(m^3)
V_t	Volume of individual tubes	(m^3)
V_{top}	Liquid volume in the top section	(m^3)
V_{bot}	Liquid volume in bottom section	(m^3)
V'	Volumetric ratio between tube-side and shell-side	(−)
We	Weber number	(−)
τ	Tortuosity of the porous wall of stainless steel tubes	(−)

ξ	The open void fraction of the porous wall of filter tubes (20%)	(−)
δ	The wall thickness of the filter tubes (2.5mm)	(−)
ε_v s	Overall gas holdup in the tube-side compartment	(−)
ε_r	Gas holdup in individual risers	(−)
ε_d	Gas holdup in individual downcomers	(−)
ρ_L	Liquid density	(kgm^{-3})
μ_{ap}	Apparent viscosity	(Pa s)
μ_L	Liquid viscosity	(Pa s)
ϕ_L^2	Two-phase friction multiplier	(−)

REFERENCES

Al-Masry, W. A. (2004). "Influence of gas separator and scale-up on the hydrodynamics of external loop circulating bubble columns." *Chemical Engineering Research & Design*, 82(A3), 381-389.

Al-Masry, W. A., and Abasaeed, A. E. (1998). "On the scale-up of external loop airlift reactors: Newtonian systems." *Chemical Engineering Science*, 53(24), 4085-4094.

Baker, O. (1954). "Simultaneous flow of oil and gas." *Oil Gas Journal*, 53, 185.

Bakker, W., Knitel, J. T., Tramper, J., and Degooijer, C. D. (1994). "Sucrose Conversion by Immobilized Invertase in a Multiple Airlift-Loop Bioreactor." *Biotechnology Progress*, 10(3), 277-283.

Bello, R. A., Robinson, C. W., and Mooyoung, M. (1984). "Liquid Circulation and Mixing Characteristics of Airlift Contactors." *Canadian Journal of Chemical Engineering*, 62(5), 573-577.

Bello, R. A., Robinson, C. W., and Mooyoung, M. (1985). "Gas Holdup and Overall Volumetric Oxygen-Transfer Coefficient in Airlift Contactors." *Biotechnology and Bioengineering*, 27(3), 369-381.

Bello, R. A., Robinson, C. W., and Mooyoung, M. (1985a). "Prediction of the Volumetric Mass-Transfer Coefficient in Pneumatic Contactors." *Chemical Engineering Science*, 40(1), 53-58.

Bendjaballah, N., Dhaouadi, H., Poncin, S., Midoux, N., Hornut, J. M., and Wild, G. (1999). "Hydrodynamics and flow regimes in external loop airlift reactors." *Chemical Engineering Science*, 54(21), 5211-5221.

Bentifraouine, C., Xuereb, C., and Riba, J. P. (1997a). "Effect of gas liquid separator and liquid height on the global hydrodynamic parameters of an external loop airlift contactor." *Chemical Engineering Journal*, 66(2), 91-95.

Bentifraouine, C., Xuereb, C., and Riba, J. P. (1997b). "An experimental study of the hydrodynamic characteristics of external loop airlift contactors." *Journal of Chemical Technology and Biotechnology*, 69(3), 345-349.

Benyahia, F., and Jones, L. (1997). "Scale effects on hydrodynamic and mass transfer characteristics of external loop airlift reactors." *Journal of Chemical Technology and Biotechnology*, 69(3), 301-308.

Binder, R. C. (1973). *Fluid Mechanics*, Englewood Cliffs, NJ.

Boyer, C., Duquenne, A. M., and Wild, G. (2002). "Measuring techniques in gas-liquid and gas-liquid-solid reactors." *Chemical Engineering Science*, 57(16), 3185-3215.

Camarasa, E., Carvalho, E., Meleiro, L. A. C., Maciel, R., Domingues, A., Wild, G., Poncin, S., Midoux, N., and Bouillard, J. (2001a). "Development of a complete model for an air-lift reactor." *Chemical Engineering Science*, 56(2), 493-502.

Camarasa, E., Carvalho, E., Meleiro, L. A. C., Maciel, R., Domingues, A., Wild, G., Poncin, S., Midoux, N., and Bouillard, J. (2001b). "A hydrodynamic model for air-lift reactors." *Chemical Engineering and Processing*, 40(2), 121-128.

Chen, M. J., Zhang, Z., and Bott, T. R. (2005). "Effects of operating conditions on the adhesive strength of Pseudomonas fluorescens biofilms in tubes." *Colloids and Surfaces B-Biointerfaces*, 43(2), 61-71.

Cheng, H., Hills, J. H., and Azzopardi, B. J. (2002). "Effects of initial bubble size on flow pattern transition in a 28.9 mm diameter column." *International Journal of Multiphase Flow*, 28(6), 1047-1062.

Chisti, M. Y., Moo-Young, M. (1987). "Airlift reactors: characteristics, applications and design considerations." *Chemical Engineering Communication*(60), 195–242.

Chisti, Y. (1989). *Airlift Bioreactors*, Elsevier, London.

Chisti, Y. (1998). "Pneumatically agitated bioreactors in industrial and environmental bioprocessing: Hydrodynamics, hydraulics and transport phenomena." *Appl. Mech. Rev.*, 51, 33-112.

Chisti, Y. (2005). "Mass transfer." Kirk-Othmer Encyclopedia of Chemical Technology, New York, 1-75.

Chisti, Y., Fujimoto, K., and Moo-Young, M. (1987). "Hydrodynamic and oxygen mass transfer studies in bubble columns and airlift bioreactors." *in Biotechnology Processes: Scale-up and Mixing, Ho, C. S., Oldshue, J. Y., eds, American Institute of Chemical Engineers, New York*, 72-81.

Choi, K. H. (2002). "Effect of unaerated liquid height on hydrodynamic characteristics of an external-loop airlift reactor." *Chemical Engineering Communications*, 189(1), 23-39.

Choi, K. H., and Lee, W. K. (1993). "Circulation Liquid Velocity, Gas Holdup and Volumetric Oxygen-Transfer Coefficient in External-Loop Airlift Reactors." *Journal of Chemical Technology and Biotechnology*, 56(1), 51-58.

Cockx, A., Line, A., Roustan, M., DoQuang, Z., and Lazarova, V. (1997). "Numerical simulation and physical modeling of the hydrodynamics in an air-lift internal loop reactor." *Chemical Engineering Science*, 52(21-22), 3787-3793.

Couvert, A., Roustan, M., and Chatellier, P. (1999). "Two-phase hydrodynamic study of a rectangular air-lift loop reactor with an internal baffle." *Chemical Engineering Science*, 54(21), 5245-5252.

Di Felice, R. (2005). "Liquid circulation rates in two- and three-phase external airlift reactors." *Chemical Engineering Journal*, 109(1-3), 49-55.

Doran, P. M. (1995). *Bioprocess Engineering Principles*, Academic Press, San Diego, California.

Du, G. C., and Yu, J. (2002). "Green technology for conversion of food scraps to biodegradable thermoplastic polyhydroxyalkanoates." *Environmental Science & Technology*, 36(24), 5511-5516.

Fadavi, A., and Chisti, Y. (2005). "Gas-liquid mass transfer in a novel forced circulation loop reactor." *Chemical Engineering Journal*, 112(1-3), 73-80.

Freitas, C., Fialova, M., Zahradnik, J., and Teixeira, J. A. (1999). "Hydrodynamic model for three-phase internal- and external-loop airlift reactors." *Chemical Engineering Science*, 54(21), 5253-5258.

Freitas, C., Fialova, M., Zahradnik, J., and Teixeira, J. A. (2000). "Hydrodynamics of a three-phase external-loop airlift bioreactor." *Chemical Engineering Science*, 55(21), 4961-4972.

Gavrilescu, M., and Tudose, R. Z. (1995). "Study of the Liquid Circulation Velocity in External-Loop Airlift Bioreactors." *Bioprocess Engineering*, 14(1), 33-39.

Gavrilescu, M., and Tudose, R. Z. (1998). "Hydrodynamics of non-Newtonian liquids in external-loop airlift bioreactors Part 2: Study of the liquid circulation velocity." *Bioprocess Engineering*, 18(2), 83-89.

Geankoplis, C. J. (2004). *Transport processes and separation process principles (includes unit operations)*, Prentice-Hall, Inc.

Glennon, B., Almasry, W., Macloughlin, P. F., and Malone, D. M. (1993). "Hydrodynamic Modeling in an Airlift-Loop Reactor." *Chemical Engineering Communications*, 121, 181-192.

Guet, S., and Ooms, G. (2006). "Fluid mechanical aspects of the gas-lift technique." *Annual Review of Fluid Mechanics*, 38, 225-249.

Guet, S., Ooms, G., Oliemans, R. V. A., and Mudde, R. F. (2003). "Bubble injector effect on the gaslift efficiency." *Aiche Journal*, 49(9), 2242-2252.

Heijnen, J. J., Hols, J., vanderLans, R., vanLeeuwen, H., Mulder, A., and Weltevrede, R. (1997). "A simple hydrodynamic model for the liquid circulation velocity in a full-scale two- and three-phase internal airlift reactor operating in the gas recirculation regime." *Chemical Engineering Science*, 52(15), 2527-2540.

Hensirisak, P. (1997). "Scale-up the use of a microbubble dispersion to increase oxygen transfer in aerobic fermentation of baker's yeast," Virginia Polytechnic Institute and State University, Blacksburg, Virginia.

Hewitt, G. F., and Roberts, D. N. (1969). "Studies of two-phase flow patterns by simultaneous X-ray and flash photography." *UKAEA Report AERE*, M2159.

Hills, J. H. (1976). "The operation of a bubble column at high throughputs I. Gas holdup measurements." *Chemical Engineering Journal*, 12, 89-99.

Hwang, S. J., and Cheng, Y. L. (1997). "Gas holdup and liquid velocity in three-phase internal-loop airlift reactors." *Chemical Engineering Science*, 52(21-22), 3949-3960.

Joshi, J. B., Ranade, V. V., Gharat, S. D., and Lele, S. S. (1990). "Sparged Loop Reactors." *Canadian Journal of Chemical Engineering*, 68(5), 705-741.

Kawagoe, M., and Robinson, C. W. (1980). "Characteristics of airlift column with external liquid circulation." Autumn Meeting of Chemical Engineers, Yokohama National University, Yokohama, Japan.

Kawase, Y., and Hashimoto, N. (1996). "Gas hold-up and oxygen transfer in three-phase external-loop airlift bioreactors: Non-Newtonian fermentation broths." *Journal of Chemical Technology and Biotechnology*, 65(4), 325-334.

Lefrancois, M. H., Mariller, C. C. and Mijane, J. V. (1955). "Effectiomements aux Proceds de Cultures forgiques et de Fermentations Industrielles." *Brevet d'Invention*, No.1, 102-200.

Liu, Y. M., Liu, Z., Mu, K., and Yuan, N. J. (2000). "Liquid circulation in a multi-tube air-lift loop reactor." *Chinese Journal of Chemical Engineering*, 8(3), 267-271.

Lu, W. J., Hwang, S. J., and Chang, C. M. (1995). "Liquid Velocity and Gas Holdup in 3-Phase Internal Loop Airlift Reactors with Low-Density Particles." *Chemical Engineering Science*, 50(8), 1301-1310.

Merchuk, J. C., Ladwa, N., Cameron, A., Bulmer, M., Berzin, I., and Pickett, A. M. (1996). "Liquid flow and mixing in concentric tube air-lift reactors." *Journal of Chemical Technology and Biotechnology*, 66(2), 174-182.

Mishima, K., and Ishii, M. (1984). "Flow Regime Transition Criteria for Upward 2-Phase Flow in Vertical Tubes." *International Journal of Heat and Mass Transfer*, 27(5), 723-737.

Mohanty, K., Das, D., and Biswas, M. N. (2006). "Hydrodynamics of a novel multi-stage external loop airlift reactor." *Chemical Engineering Science*, 61(14), 4617-4624.

Nicol, R. S., and Davidson, J. F. (1988). "Gas holdup in circulating bubble columns." *Transactions of the Institution of Chemical Engineers, A:Chemical Engineering Research and Design*, 68, 152-158.

Nikakhtari, H., and Hill, G. A. (2005). "Hydrodynamic and oxygen mass transfer in an external loop airlift bioreactor with a packed bed." *Biochemical Engineering Journal*, 27(2), 138-145.

Nishikawa, M., Kato, H., and Hashimoto, K. (1997). "Heat transfer in aerated tower filled with non-Newtonian liquid." *Ind. Eng. Chem. Process Des. Develop.*, 16, 133137.

Onken, U., and Weiland, P. (1980). "Hydrodynamics and mass transfer in an airlift loop fermentor." *Eur. J. Appl. Microbiol. Biotechnol.*, 10, 31-40.

Patel, T. D., and Bott, T. R. (1991). "Oxygen Diffusion through a Developing Biofilm of Pseudomonas-Fluorescens." *Journal of Chemical Technology and Biotechnology*, 52(2), 187-199.

Petersen, E. E., and Margaritis, A. (2001). "Hydrodynamic and mass transfer characteristics of three-phase gaslift bioreactor systems." *Critical Reviews in Biotechnology*, 21(4), 233-294.

Popovic, M., and Robinson, C. W. (1984). "Estimation of some important design parameters for non-Newtonian liquids in pneumatically-agitated fermenters." *Proceedings of the 34th Canadian Chemical Engineering Coference*, 30th September - 3rd October, Quebec City, 258-263.

Popovic, M., and Robinson, C. W. (1988). "External-Circulation-Loop Airlift Bioreactors - Study of the Liquid Circulating Velocity in Highly Viscous Non-Newtonian Liquids." *Biotechnology and Bioengineering*, 32(3), 301-312.

Rubio, F. C., Garcia, J. L., Molina, E., and Chisti, Y. (2001). "Axial inhomogeneities in steady-state dissolved oxygen in airlift bioreactors: predictive models." *Chemical Engineering Journal*, 84(1), 43-55.

Saez, A. E., Marquez, M. A., Roberts, G. W., and Carbonell, R. G. (1998). "Hydrodynamic model for gas-lift reactors." *Aiche Journal*, 44(6), 1413-1423.

Samaras, V. C., and Margaris, D. P. (2005). "Two-phase flow regime maps for air-lift pump vertical upward gas-liquid flow." *International Journal of Multiphase Flow*, 31(6), 757-766.

Song, C. H., No, H. C., and Chung, M. K. (1995). "Investigation of Bubble Flow Developments and Its Transition Based on the Instability of Void Fraction Waves." *International Journal of Multiphase Flow*, 21(3), 381-404.

Sotiriadis, A. A., Thorpe, R. B., and Smith, J. M. (2005). "Bubble size and mass transfer characteristics of sparged downwards two-phase flow." *Chemical Engineering Science*, 60(22), 5917-5929.

Swamee, P. K., and Jain, A. K. (1976). "explicit equations for pipe-flow problems." *Journal of the hydraulics division*, 102(HY5), 657-664.

Taitel, Y., Bornea, D., and Dukler, A. E. (1980). "Modelling flow pattern transitions for steady upward gas-liquid flow in vertical tubes." *AIChE Journal*, 26(3), 345-354.

Vera, L., Delgado, S., and Elmaleh, S. (2000). "Dimensionless numbers for the steady-state flux of

cross-flow microfiltration and ultrafiltration with gas sparging." *Chemical Engineering Science*, 55(17), 3419-3428.

Verlaan, P., Vaneijs, A. M. M., Tramper, J., Vantriet, K., and Luyben, K. (1989). "Estimation of Axial-Dispersion in Individual-Sections of an Airlift-Loop Reactor." *Chemical Engineering Science*, 44(5), 1139-1146.

Vial, C., Poncin, S., Wild, G., and Midoux, N. (2002). "Experimental and theoretical analysis of the hydrodynamics in the riser of an external loop airlift reactor." *Chemical Engineering Science*, 57(22-23), 4745-4762.

Wallis, G. B. (1969). *One Dimensional Two Phase Flow*, McGraw-Hill, New York.

Yang, S.-t. (2006). *Bioprocessing for Value-added Products from Renewable Resources: New Technologies And Applications*, Elsevier Science Ltd.

Yu, J., Ji, M., and Yue, P. L. (1999). "A three-phase fluidized bed reactor in the combined anaerobic/aerobic treatment of wastewater." *Journal of Chemical Technology and Biotechnology*, 74(7), 619-626.

Yu, J., and Si, Y. T. (2001). "Dynamic study and modeling on formation of polyhydroxyalkanoates coupled with treatment of high strength wastewater." *Environmental Science & Technology*, 35, 3584-3588.

Zuber, N., and Findlay, J. A. (1965). "Average Volumetric, Concentration in Two-Phase Flow Systems." *Journal of Heat Transfer*, 87, 453-468.

Appendix A. Measurement of gas holdup in the riser(s)

Inclined U-tube was used to measure the gas holdup in the riser(s) of MAMBR, the theory of this measurement is explained as follows:

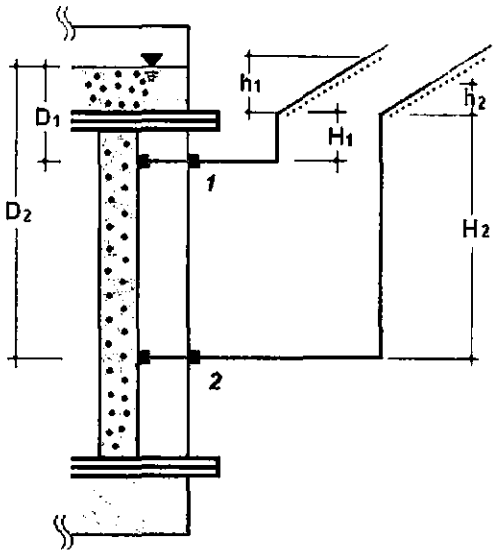

Fig. A1. Schematic diagram of the measurement of inclined U-tube.

For pressure at position 1:

$$P_1 = P_{atm} + \rho_D g D_1 = \rho_L g(h_1+H_1) + P_{atm} \qquad \text{(A1)}$$

For pressure at position 2:

$$P_2 = P_{atm} + \rho_D g D_2 = \rho_L g(h_2+H_2) + P_{atm} \qquad \text{(A2)}$$

Then, $P_1 - P_2 = \rho_D g(D_2-D_1) = \rho_L g[(H_2 - H_1)+(h_2-h_1)]$ (A3)

Let $D_2 - D_1 = H_2 - H_1 = \Delta H$, and $h_1 - h_2 = \Delta h$

After rearranging, Eq. A3 becomes,

$$\rho_D = \rho_L (1 - \Delta h / \Delta H) \qquad \text{(A4)}$$

For gas-liquid mixture, the dispersion density ρ_D can be expressed as:

$$\rho_D = \rho_L (1 - \varepsilon_r) + \rho_G \varepsilon_r \qquad \text{(A5)}$$

ρ_G is negligible when it is compared with ρ_L, therefore Eq.A5 can be further simplified as:

$$\rho_D = \rho_L (1 - \varepsilon_r) \qquad \text{(A6)}$$

Equating Eq. A4 to A6, it gives:

$$\varepsilon_r = \Delta h / \Delta H \qquad \text{(A7)}$$

Appendix B. Prepiction of diffusivity of organic acids in water

For small solute molar volumes, a semi-theoretical expression was proposed by Geankoplis (2004), which is used for most general purposes where in the solute (A, e.g. lactic or acetic acid) is dilute in the solvent (B, e.g. water):

$$D_{AB} = 1.173\times10^{-16}(\phi \cdot M_B)^{1/2}\frac{T}{\mu_B V_A^{0.6}} \qquad \text{(B.1)}$$

ϕ: Association parameter of the solvent equals 2.6 for water.

M_B: the molecular weight of solvent B, for water, equals 18.02kg *mass/kg mol.*

μ_B: the viscosity of B in *kg/m·s.*

For water, At room temperature, 22 °C, μ_B=0.9579×10^{-3} *kg/m·s*

under heating status, at 32 °C, μ_B=0.7697×10^{-3} *kg/m·s*

V_A: the solute molar volume at the boiling point

T: temperature in *K.*

For lactic acid solvent ($C_3H_6O_3$) from table 6.3-2 (Geankoplis 2004)

V_A =3(0.0148) +6(0.0037) + [2(0.012) +1(0.0074)] =0.0980 m^3kgmol

Substituting above parameters into diffusivity prediction equation:

$$D_{AB,22°C} = 1.173\times10^{-16}(2.6\times18.02)^{1/2}\frac{295}{(0.9579\times10^{-3})(0.0980)^{0.6}} = 9.964\times10^{-10}m^2/s$$

$$D_{AB,32^{\circ}C} = 1.173\times10^{-16}(2.6\times18.02)^{1/2}\frac{305}{(0.7697\times10^{-3})(0.0980)^{0.6}} = 1.28\times10^{-9}\,m^2/s$$

Similarly, for acetic acid solvent ($C_2H_4O_2$) at 22 °C:

$$D_{\text{acetic acid in water},22^{\circ}C} = 1.173\times10^{-16}(2.6\times18.02)^{1/2}\frac{295}{(0.9579\times10^{-3})(0.0638)^{0.6}} = 1.289\times10^{-9}\,m^2/s$$

Appendix C. Measurement of Diffusivity of organic Acids in Water

Mineral solution:

20L, sterilized 210°C, 0.15MPa, for 15 minutes, collecting at 60~75 °C

Ingredients:

NaH_2PO_4	2.0g/L×20L=40g
K_2HPO_4	2.8g/L×20L=56g
$MgSO_4 \cdot 7H_2O$	0.5g/L×20L=10g
$NaHCO_3$	0.5g/L×20L=10g
$CaCl_2 \cdot 2H_2O$	0.01g/L×20L=0.2g
$(NH4)_2SO_4$	5g/L×20L=100g
Trace Solution	5ml/L×20L=100ml
Ferric Ammonia Citrate	0.05g/L×20L=1.0g

YPM:

Yeast extracts (Y)	10g/L
Peptone (P)	10g/L
Meat extracts (M)	5g/L
Ammonium sulfate (providing N for the bacteria)	5g/L
Glucose (providing C for the bacteria)	10g/L

Experimental data, which were used to calculate the diffusivity of organic acids in water, are collected and summarized in Table C.1.

Table C.1. Experimental data of Measurement of Diffusivity of organic Acids in water

Gas flow rate: 3-riser, at U_{Gr} = 0.05m/s							
Sampling Time (hours)		Shell-side concentration C_s (10^{-3} kg mol/m^3)		Tube-side concentration C_t (10^{-3} kg mol/m^3)		Turbidity OD (—)	Experimental conditions
		Lactic acid	Acetic acid	Lactic acid	Acetic acid		
1	0	186.56	104.50	6.17	3.69	0.266	PH 6.73; 22.1°C; DO 84.5
2	1.95	235.67	140.67	7.64	4.38	0.260	PH 6.67; 21.8°C; DO 84.5
3	3.95	229.98	128.67	9.19	5.60	0.259	PH 6.61; 21.5°C; DO 84.3
4	5.95	233.33	130.00	10.14	5.88	0.265	PH 6.56; 21.3°C; DO 84.1
5	7.95	231.11	128.50	11.56	7.00	0.266	PH 6.51; 21.1°C; DO 84.0
6	9.95	232.22	127.50	12.56	7.33	0.265	PH 6.46; 21.0°C; DO 83.9
7	11.95	231.11	129.50	14.67	8.50	0.266	PH 6.40; 20.9°C; DO 83.8
8	14.70	216.89	105.00	15.89	9.67	0.269	PH 6.32; 20.6°C; DO 83.6
9	16.20	227.78	127.00	16.89	10.23	0.268	PH 6.28; 20.8°C; DO 83.7
10	18.03	221.11	122.67	18.43	10.90	0.299	PH 6.22; 20.6°C; DO 83.5
11	20.11	223.89	106.33	19.62	11.00	0.310	PH 6.16; 20.8°C; DO 82.9
12	22.11	226.67	122.00	20.94	11.67	0.349	PH 6.11; 20.6°C; DO 81.4
13	24.11	—	—	22.33	11.43	0.398	PH 6.08; 20.7°C; DO 80.2
14	26.11	—	—	24.04	12.30	0.481	PH 6.07; 20.6°C; DO 78.7
15	28.11	—	—	26.40	10.32	0.656	PH 6.12; 20.6°C; DO 77.6
16	31.11	—	—	25.71	8.35	0.840	PH 6.18; 20.9°C; DO 77.8
17	34.11	—	—	24.78	4.62	1.018	PH 6.28; 20.9°C; DO 75.8
18	37.11	—	—	25.58	5.03	1.370	PH 6.44; 21.0°C;

							DO 74.6
19	40.11	—	—	21.44	4.92	1.952	PH 6.67; 21.2°C; DO 67.2
20	43.11	—	—	13.22	5.22	2.760	PH 6.78; 21.6°C; DO 63.3
21	46.11	—	—	2.88	5.22	3.420	PH 6.97; 21.9°C; DO 61.2
22	48.11	215.22	115.17	1.58	4.33	3.900	PH 7.00; 22.5°C; DO 69.9